

MECHANICAL BEHAVIOUR OF BOLTED JOINTS UNDER IMPACT RATES OF
LOADING

By

Andrew Vander Klok

UNCLASSIFIED: Distribution Statement A. Approved for public release

A THESIS

Submitted to
Michigan State University
in partial fulfillment of the requirements
for the degree of

MASTER OF SCIENCE

Mechanical Engineering

2012

Report Documentation Page

Form Approved
OMB No. 0704-0188

Public reporting burden for the collection of information is estimated to average 1 hour per response, including the time for reviewing instructions, searching existing data sources, gathering and maintaining the data needed, and completing and reviewing the collection of information. Send comments regarding this burden estimate or any other aspect of this collection of information, including suggestions for reducing this burden, to Washington Headquarters Services, Directorate for Information Operations and Reports, 1215 Jefferson Davis Highway, Suite 1204, Arlington VA 22202-4302. Respondents should be aware that notwithstanding any other provision of law, no person shall be subject to a penalty for failing to comply with a collection of information if it does not display a currently valid OMB control number.

1. REPORT DATE

07 NOV 2012

2. REPORT TYPE

Masters Thesis

3. DATES COVERED

01-01-2012 to 01-11-2012

4. TITLE AND SUBTITLE

**MECHANICAL BEHAVIOUR OF BOLTED JOINTS UNDER
IMPACT RATES OF LOADING**

5a. CONTRACT NUMBER

W56hzv-07-2-0001

5b. GRANT NUMBER

5c. PROGRAM ELEMENT NUMBER

6. AUTHOR(S)

Andrew Klok

5d. PROJECT NUMBER

5e. TASK NUMBER

5f. WORK UNIT NUMBER

7. PERFORMING ORGANIZATION NAME(S) AND ADDRESS(ES)

**Michigan State University, 450 Administration Bldg, Department of
Mechanical Engineering, Warren, Mi, 48824**

8. PERFORMING ORGANIZATION REPORT
NUMBER

; #23440

9. SPONSORING/MONITORING AGENCY NAME(S) AND ADDRESS(ES)

**U.S. Army TARDEC, 6501 East Eleven Mile Rd, Warren, Mi,
48397-5000**

10. SPONSOR/MONITOR'S ACRONYM(S)

TARDEC

11. SPONSOR/MONITOR'S REPORT
NUMBER(S)

#23440

12. DISTRIBUTION/AVAILABILITY STATEMENT

Approved for public release; distribution unlimited

13. SUPPLEMENTARY NOTES

14. ABSTRACT

Bolted joints are extensively used in many automotive and aeronautical sectors where two members are bolted together. This particular method of fastening is vastly used in many industrial disciplines as it serves as an easy and non-destructive method to join and subsequently disassemble a complex structure. Since, bolted joints constitute an integral part of many structural components, this directly implicates the necessity to investigate the mechanical response of the bolted joints under a variety of loading rates to ensure structural integrity. Existing literature exists addressing bolted joint failure for a myriad of different geometrical configurations, and identifies the key parameters associated with it; for instance, non-dimensional ratios between width of the joint (w), edge distance (e), diameter of the hole/bolt (d) and thickness of the joint (t). However, very limited literature exists addressing the structural integrity of these joints if subjected to time-dependent loading conditions (for example, impact). The present study aims at investigating dynamic mechanical behavior of bolted joints and the role of the non-dimensional parameters affecting joint failure. The Split Hopkinson Pressure Bar technique has been employed to characterize bolted joint failure under impact rates of loading for both compression and tensile loading conditions. Hole elongation and buckling are the key modes of failure under dynamic compressive loading conditions, whereas tear-out, tension, and cleavage failure constitutes the predominant failure modes under dynamic tensile loading conditions. Aluminum-Aluminum and Aluminum-Glass fiber reinforced composite bolted joints were tested under dynamic compression and tension respectively. An experimental method was developed for measuring and monitoring the response to the bolt preload during impact. It was determined that the asymptotic region of failure shifts from static to dynamic loading conditions.

15. SUBJECT TERMS					
16. SECURITY CLASSIFICATION OF:			17. LIMITATION OF ABSTRACT	18. NUMBER OF PAGES	19a. NAME OF RESPONSIBLE PERSON
a. REPORT unclassified	b. ABSTRACT unclassified	c. THIS PAGE unclassified	Public Release	83	

ABSTRACT

Mechanical Behavior of Bolted Joints Under Impact Rates of Loading

Andrew Vander Klok

Bolted joints are extensively used in many automotive and aeronautical sectors where two members are bolted together. This particular method of fastening is vastly used in many industrial disciplines as it serves as an easy and non-destructive method to join and subsequently disassemble a complex structure. Since, bolted joints constitute an integral part of many structural components, this directly implicates the necessity to investigate the mechanical response of the bolted joints under a variety of loading rates to ensure structural integrity. Existing literature exists addressing bolted joint failure for a myriad of different geometrical configurations, and identifies the key parameters associated with it; for instance, non-dimensional ratios between width of the joint (w), edge distance (e), diameter of the hole/bolt (d) and thickness of the joint (t). However, very limited literature exists addressing the structural integrity of these joints if subjected to time-dependent loading conditions (for example, impact). The present study aims at investigating dynamic mechanical behavior of bolted joints and the role of the non-dimensional parameters affecting joint failure. The Split Hopkinson Pressure Bar technique has been employed to characterize bolted joint failure under impact rates of loading for both compression and tensile loading conditions. Hole elongation and buckling are the key modes of failure under dynamic compressive loading conditions, whereas tear-out, tension, and cleavage failure constitutes the predominant failure modes under dynamic tensile loading conditions. Aluminum-Aluminum and Aluminum-Glass fiber reinforced composite bolted joints were tested under dynamic compression and tension respectively. An experimental method was developed for measuring and monitoring the response to the bolt preload during impact. It was determined that the asymptotic region of failure shifts from static to dynamic loading conditions.

Acknowledgements

The author would like to express his gratitude to Dr. Srinivasan Arjun Tekalur for his guidance and support in all works accomplished. The author would also like to show appreciation to Dr. Gary Cloud, Michigan State University for their valuable suggestions and help in various parts of the current research. In addition to this, the author thanks Wei Zhang and Abhishek Dutta for producing an enjoyable environment in the laboratory. The author acknowledges the support and help of Gail Berry, Mike McLean, Adam Klein and Todd for their help throughout the research work.

Table of Contents

List of Tables

List of Figures

List of Symbols

1. Background of Bolted Joint Analysis

1.1 Joint Member Stiffness

1.2 Bolt Pretension Characteristics

1.3 Background to the Kolsky Pressure Bar Technique Application to Bolted Joints

1.4 References

2. Evaluating Monolithic and Bolted Joint Behavior at high Strain Rates in a Split Hopkinson Pressure Bar

2.1 Abstract

2.2 Introduction to Monolithic Joints

2.3 Materials and Methods

2.4 Results

2.5 Discussion

2.6 Recommendations and Conclusion

2.7 References

3. Evaluating Bolted Joint Behavior at High Strain Rates

3.1 Abstract

3.2 Introduction to Bolted Joints

3.3 Materials and Methods

3.4 Results and Discussion

3.5 Effect of Slip

3.6 Effect of Joint Pre-load

3.7 Conclusion

3.8 References

4. Metal to Composite Bolted Joint Behavior Evaluated at Impact Rates of Loading

4.1 Abstract

4.2 Introduction to Dissimilar Material Fastening

4.3 Materials and Methods

4.4 Results and Discussion of Failure Modes Observed

4.5 Specimen Static Load Bearing Characteristics

4.6 Specimen Dynamic Load Bearing Characteristics

4.7 Failure modes of Static and Dynamically Loaded Bolted Joints

4.8 Conclusion

4.9 References

5. Conclusion

5.1 Concluding Remarks

5.2 Future Scope of Work

Appendix A Wire and Strain Gage Installation Notes

Appendix B Trigger Mechanisms and Phantom High Speed Camera

Appendix C Ectron 513-2A Amplifier and Calibration Notes

List of Tables

- Table 2.1** Geometric Parameters for experimental monolithic specimen testing
- Table 2.2** Geometric Parameters for Finite Element monolithic specimen testing
- Table 3.1** Specimen geometry and set preload for specimens tested in uniaxial compression in the SHPB.
- Table 4.1** Specimen non-dimensional parameters
- Table 4.2** Summary of failure mode time initiation
- Table AC1** Characterization of bridge configuration and sensitivity, where better sensitivity signifies a smaller ratio of $\mu\epsilon/\text{Volt}$

List of Figures

- Figure 1.1** Description of varying bolt regions [Bickford, 1990]
- Figure 1.2** Exaggerated view of bolt and member deformation during bolt preloading [Farahmand, 2001]
- Figure 1.3** General physical setup of the SHPB where striker impacts pulse shaper at velocity (V)
- Figure 2.1** Show the ABAQUS model with specimen 7a ready to be tested on the right and the experimental setup on the left. The specimen can be seen between the incident and transmission bars.
- Figure 2.2** Geometrical definitions for monolithic specimen size descriptions
- Figure 2.3** Loading rate from transmitted force of specimen for varying e/d in compression. Experimental error bars are calculated with 95% confidence interval
- Figure 2.4** The amount of time it takes the specimen to first reach equilibrium for varying e/d in compression. Experimental error bars are calculated with 95% confidence interval
- Figure 2.4** The amount of time it takes the specimen to first reach equilibrium for varying e/d in compression. Experimental error bars are calculated with 95% confidence interval
- Figure 2.5** Total amount of time the specimen is at equilibrium for varying e/d in compression. Experimental error bars are calculated with 95% confidence interval
- Figure 2.6** Samples that have been bent due to testing. All samples were visually inspected against a flat surface to determine if permanent deformation due to bending has occurred
- Figure 2.7** Loading rate in MN/s for varying l/d , w/d , and $d/t=1.0$ and 0.5
- Figure 2.8** Specimen equilibrium start time for varying l/d , w/d , and $d/t=1.0$
- Figure 2.9** Specimen equilibrium start time for varying l/d , w/d , and $d/t=0.5$
- Figure 2.10** Specimen total time spent at equilibrium during loading for varying l/d , w/d , and $d/t=1.0$
- Figure 2.11** Specimen total time spent at equilibrium during loading for varying l/d , w/d , and $d/t=0.5$

- Figure 3.1** Schematic of the SHPB apparatus used in current investigation. Zoomed in view of specimen region shows the placement of the load cell to monitor bolt pre-load.
- Figure 3.2** Load cell calibration for bolt diameters of 0.25” and 0.188”.
- Figure 3.3** Plot of pulses obtained in incident and transmission bars. Shown in the lower right is the bolted joint sandwiched within the SHPB incident and transmission bars.
- Figure 3.4** High speed images of bolted joint slipping. Scale bar represents 0.125 inches and white reference line correlates to slip initiation at 16 μ s.
- Figure 3.5** Plot of transmitted force versus time: (a) initial loading, (b) joint slip, (c) post joint slip loading, and (d) unloading.
- Figure 3.6** Loading rate vs. Force transmitted of specimen during slip for varying pre-loads.
- Figure 3.7** Plot of maximum bearing stress versus pre-load of bolt for varying geometries where specimen ID# represent the geometrical parameters as listed in **Table 1**.
- Figure 3.8** Plot of loading rate versus pre-load of bolt for varying geometries where specimen ID# represent the geometrical parameters as listed in **Table 1**.
- Figure 3.9** Strain time curves from the 0.25” load cell at pre-loads of 0lbf, 100lbf, 300lbf, 500lbf, 700lbf, and monolithic base test.
- Figure 4.1** Split Hokinson tension bar apparatus setup (top) and the specimen setup with holding fixtures (bottom)
- Figure 4.2** Possible Failure modes of a loaded bolted joint loaded at the hole
- Figure 4.3** Bearing stress vs. displacement curves for bolted joints tested in tension at 1.5mm/min with region 1, 2, and 3 respectively correlating to initial loading, slip, and bearing load to failure.
- Figure 4.4** static and impact loaded samples compared with maximum bearing stress before catastrophic failure
- Figure 4.5** Rate of load transfer to the composite bolted joint
- Figure 4.6** Load transfer curve and correlating failure mode images for the metal composite joints tested with $e/d=1.0$
- Figure 4.7** Load transfer curve and correlating failure mode images for the metal composite joints tested with $e/d=2.0$
- Figure 4.8** Load transfer curve and correlating failure mode images for the metal composite joints tested with $e/d=3.0$

- Figure 4.9** Load transfer curve and correlating failure mode images for the metal composite joints tested with $e/d=4.0$
- Figure 4.10** Asymptotic failure behavior of bolted joints loaded in tension
- Figure AB1** Flow schematic of equipment for Hopkinson bar data acquisition and high speed capture calibration
- Figure AC1** 1/2-Wheatstone bridge circuit
- Figure AC2** 1/2-Wheatstone bridge Hopkinson incident bar schematic, where numbers in triangles represent pin connection in Ectron 513-2A enclosure
- Figure AC3** Full Wheatstone bridge circuit
- Figure AC4** Full Wheatstone bridge Hopkinson transmission bar and load cell schematic, where numbers in triangles represent pin connections in Ectron 513-2A enclosure

List of Symbols

A_d = major diameter of fastener

A_t = tensile stress area

ϵ_i = incident strain

ϵ_r = reflected strain

ϵ_t = transmitted strain

E = youngs modulus of elasticity

F = force applied

F_g = Strain gage factor

k_b = Effective stiffness of bolt

k_t = stiffness of threaded portion of bolt

k_d = stiffness of unthreaded portion of bolt

k_m = effective stiffness of joint members

k_i = stiffness of individual members

l_t = length of threaded portion of grip

l_d = Length of unthreaded portion in grip

R_c = resistance of shunt calibration in Ohms

R_g = Resistance of gage in Ohms

σ = Stress

y = deflection of spring

Chapter 1 Background to Bolted Joint Analysis

1.1 Joint and Member Stiffness Calculations

There are many different of joints that can be utilized to connect structural parts together. Prevailing as the most dominant in most structures is the method of threaded fastener or bolt. This type of fastener is popular in that it provides a fast and easy way to attach structures together however has some drawbacks. Fastener joints can be understood to have regions of high stress concentrations where cracks can initiate to cause structural failure. In this chapter bolted joints will be discussed and an emphasis will be given to the analysis and behavior of a shear loaded bolted joint and dynamic experimental testing apparatus.

As the bolt and nut is torqued together a subsequent bolt preload or pretension is applied. This preload on the nut causes a reaction compression force to be applied to the joint subsequently holding two parts together. However due to the pretension to the bolt and reaction force of the materials used, there is some elastic deformation to the bolt and members referred to as joint and member stiffness. This idea of joint and member stiffness is comparable to that of a spring where a clear relationship between force and displacement can be related with the use of the below **equation 1.1**.

$$F = F(y) \tag{1.1}$$

Then, taking the limit of this equation as change of deflection y approaches zero yields the spring stiffness or bolt and member stiffness is shown below in **equation 1.2**.

$$k(y) = \lim_{\Delta y \rightarrow 0} \frac{\Delta F}{\Delta y} = \frac{dF}{dy} \tag{1.2}$$

Most materials used in the manufacture of a bolt or joint member operate in their elastic region a linear behavior is observed. Stiffness can be written to show that units of force by distance of

deflection will yield a stiffness constant to describe the stiffness of a bolt or joint member as shown in **Equation 1.3**. **Equation 1.3** can be further manipulated to accommodate for torsional spring rate simply by considering a torque by displacement in radians.

$$k = \frac{F}{y} \quad 1.3$$

Typically a bolt is configured into two different parts, that of the smooth shank portion and the threaded section shown in **figure 1.1**. The effective stiffness of the bolt can then be attained through the consideration that both the smooth portion and threaded portion of the bolt are in series with each other yielding **equation 1.4**.

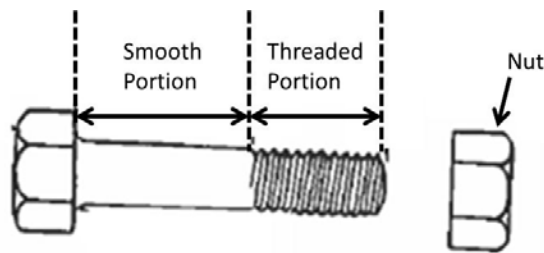


Figure 1.1 Description of varying bolt regions [Bickford, 1990]

$$\frac{1}{k_{eq}} = \frac{1}{k_1} + \frac{1}{k_2} = \frac{k_1 k_2}{k_1 + k_2} \quad 1.4$$

Considering the stiffness equation, the threaded and unthreaded portions of the bolt can be described below in **equations 1.5** and **1.6** respectively.

$$k_t = \frac{A_t E}{l_t} \quad 1.5$$

$$k_d = \frac{A_d E}{l_d} \quad 1.6$$

Substituting back into the series equation yields the total effective stiffness of a bolt shown below. It can be noted that if a bolt has a relatively small section for the threaded portion of the bolt relative to its total length, the stiffness portion of the threaded section can be ignored yielding **equation 1.7**.

$$k_b = \frac{A_d A_t E}{A_d l_t + A_t l_d} \quad 1.7$$

The clamping zone of the bolt on the members cannot be neglected as the members themselves will undergo some sort of elastic deformation due to reaction forces from setting pretension on the bolt and nut by torquing them together as seen in the below in **figure 1.2**. The figure shows an exaggerated picture of what type of deformation may occur within the members as the nut is tightened to the bolt.

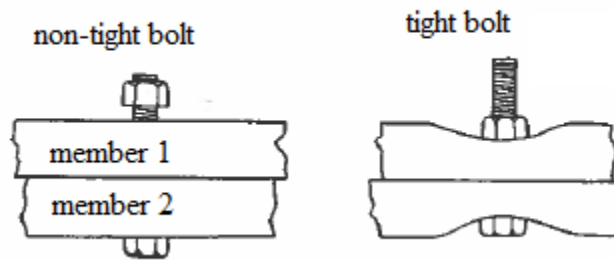


Figure 1.2 Exaggerated view of bolt and member deformation during bolt preloading

[Farahmand, 2001]

Similar to bolt stiffness the equivalent stiffness of the members are calculated with the consideration that the elastic components such as gaskets, or joint members are in series and can be simply added using the below formula **equation 1.8**. However, concern arises when there is no gasket or area to use with the calculation of the member stiffness.

$$\frac{1}{k_m} = \frac{1}{k_1} + \frac{1}{k_2} + \frac{1}{k_3} + \dots + \frac{1}{k_i}$$

1.8

1.2 Bolt pretension characteristics

Compression induced from the pretension on the bolt is not constant throughout the thickness of the member clamped; a pressure cone method will be used. This method will yield the stress distribution area of the clamped region of the bolt. This method has been refined by means of research conducted from [Ito, Toyoda, & Nagata, 1977] where an ultrasonic technique was used to determine the pressure distribution through the thickness of the material with a pretension bolt. The area of compression was reported to be cone shaped, where the compression is maximum at the top and increases in radius with reducing pressure in an outward direction away from the bolt. This pressure distribution has led to the conclusion that the compressive pressure drops dramatically after 1.5 bolt radii [Budynas & Nisbett, 2006]. This implicates that the friction force between two interfaces is greatly affected with bolt spacing and preload, drastically changing overall strength of the joint [Rowlands, Rahman, Wilkinson, & Chiang, 1982], [Park, 2001], [Yan, Wen, Chang, & Shyprykevich, 1999]. Where the strength of the bolted joint can be described as the maximum stress attained before failure and frictional forces are dependent upon bolt preload, coefficient of friction, hole clearance, and mating surfaces [Groper, 1985]. Much effort has been put fourth to examine the behavior of bolted joints evaluated at static or quasi-static strain rates, but the same cannot be said for time dependent loading conditions. The following discussion explains an experimental technique to how an impact load can be successfully imparted to a bolted joint.

1.3 Background to the split Hopkinson bar technique application to bolted joints

The split Hopkinson or Kolsky bar is a type of loading apparatus that can load a specimen to strain rates of 10^2 - 10^4 ϵ/s . The device shown in **figure 3** has three main components: the striker, incident bar, and transmission bar and proves to be a convenient dynamic loading device as it allows for the decoupling of specimen inertial and strain rate effects [**Srivastava, Shukla, & Parameswaran, 2000**]. The two bars are outfitted with strain gages and wired to a dynamic signal conditioning amplifier then to an oscilloscope for data acquisition of incident, reflected, and transmission pulses. The aim of the Kolsky bar to develop stress strain relationship at high strain rates, however for bolted joint testing is limited to load transfer as will be discussed.

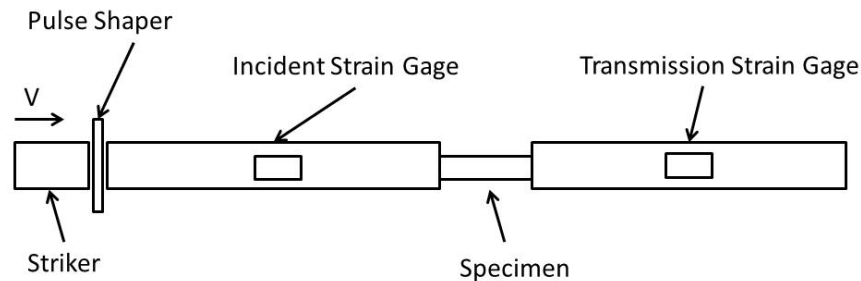


Figure 1.3 General physical setup of the SHPB where striker impacts pulse shaper at velocity

(V)

An axial impact on the incident bar is caused by firing an air gun this generates a travelling compressive wave in the incident bar. Typically, the material and the cross-section of the specimen is not the same as that of the incidence bar. Due to the mismatch of mechanical impedance of these two, when the travelling wave hits the specimen, part of the wave is reflected and part is allowed to transmit through to the specimen. Following a one-dimensional wave analysis of the incident and transmission bar from [**Shukla & Dally, 2010**] it is possible to obtain stress, displacements, and strains of at the specimen interfaces of at the bar as well as

average specimen stress and strain rate. However, this analysis works well for a small uniform specimen, but fundamental requirements for the theory to hold valid from [Chen & Song, 2009] are difficult to attain for a bolted joint specimen. Chapter 2 shows that for long monolithic specimens of varying lengths a state of equilibrium is possible to reach given that proper pulse shaping techniques as noted in [Davies & Hunter, 1963], [Frantz, Follansbee, & Wright, 1984], [Song & Chen, 2004], [Ravichandran & Subhash, 1994]. If similar methods are adapted to actual bolted joint testing such as that in Chapter 3 and 4 the transmitted force and subsequent bearing stress only can be calculated as the bolted joints tested are not uniform in cross-sectional area or material. Important failure mode dependencies and observations are observed in subsequent chapters with load vs. time data correlated with high speed images.

1.4 References

- Bickford, J. H. (1990). *An Introduction to the Design and Behavior of Bolted Joints*. New York: Marcel Dekker, Inc.
- Budynas, & Nisbett. (2006). *Shigley's Mechanical Engineering Design, Eighth Edition*. United States: McGraw-Hill.
- Chen, W., & Song, B. (2009). Kolsky Bar (SHPB) Experiments. (p. 103). SEM Preconference Short course.
- Davies, E. D., & Hunter, S. (1963). The dynamic compression testing of solids of the method of split Hopkinson pressure bar. *J. Mech. Phys. Solids*, 155–181.
- Farahmand, B. P. (2001). Fracture Mechanics for Metals, Composites, Welds, and Bolted Joints. In B. P. Farahmand, *Fracture Mechanics for Metals, Composites, Welds, and Bolted Joints* (pp. 304-322). Norwell: Kluwer Academic Publishers.
- Frantz, C., Follansbee, P., & Wright, W. (1984). New Experimental Techniques with the Split Hopkinson Pressure Bar. *8th International conference on high energy rate fabrication*.
- Groper, M. (1985). Microslip and Macroslip in Bolted Joints. *Experimental Mechanics*, 171-174.
- Ito, Y., Toyoda, J., & Nagata, S. (1977). Interface Pressure Distribution in a Bolt-Flange Assembly. *ASME*, 77-WA/DE-11.
- Park, H. (2001). Effects of stacking sequence and clamping force on the bearing strength of mechanically fastened joints in composite laminates. *Composite Structures*, 213-221.
- Ravichandran, G., & Subhash, G. (1994). Critical appraisal of limiting strain rates for compression testing of ceramics in a split Hopkinson pressure bar. *J. Am. Ceram. Soc.*, 263-267.
- Rowlands, R., Rahman, M., Wilkinson, T., & Chiang, Y. (1982). Single and multiple-bolted joints in orthotropic materials. *Composites*, 273-279.
- Shukla, A., & Dally, J. (2010). Experimental Solid Mechanics. In A. Shukla, & J. Dally, *Experimental Solid Mechanics*. Knoxville: College House Enterprises,.
- Song, B., & Chen, W. (2004). Dynamic Stress Equilibration in Split Hopkinson Pressure Bar Tests on Soft Materials. *Experimental Mechanics*, 300-312.
- Srivastava, V., Shukla, A., & Parameswaran, V. (2000). Experimental Evaluation of the Dynamic Shear Strength of Adhesive-Bonded Lap Joints. *Journal of Testing and Evaluation*, 438-442.

Yan, Y., Wen, W.-D., Chang, F. -K., & Shyprykevich, P. (1999). Experimental Study on Clamping Effects on the Tensile Strength of Composite Plates with a Bolt-Filled Hole. *Composites*, 1215-1229.

**Chapter 2 Evaluating Monolithic and Bolted Joint Behavior at High Strain Rates in a Split
Hopkinson Pressure Bar**

2.1 Abstract

The present study aims at investigating and characterizing failure of bolted-lap joints in the dynamic regime under a variety of strain rates in a Split Hopkinson Pressure Bar. The key parameters influencing the mechanical behavior of bolted joints are width of the joint (w), edge distance (e), diameter of the hole/bolt (d) and thickness of the joint (t). Extensive literature studies exist on bolted-lap joints which identify the critical values of non-dimensional parameters (typically, w/d and e/d) where failure mode of the joint undergoes a transition to various states from tension, tear-out & hole elongation. However, the above modes of failure would be prevalent under tensile loading conditions. Hole elongation and buckling are the key modes of failure under compressive loading conditions. Buckling is dependent upon the length conditions of the joint and thus, identification of critical length where strain in the joint under dynamic loading instability occurs can be considered a defining parameter under impact rates of loading. In order to better understand the mechanical response, monolithic specimens were constructed by fixing w/d and d/t while varying e/d to determine the critical length, a function of e , where buckling is initiated. Upon identification of the critical e/d ratio, w/d and d/t would be varied, subjected to geometric constraints of the bar, to determine optimum range of those parameters where failure behavior of the joint would no longer be dominated by buckling. Monolithic specimens can be visualized as ideal bolted joints and based on their outcome; they would in-turn serve as a baseline with respect to which in later studies the actual joints will be correlated and compared.

2.2 Introduction to Monolithic Joints

Bolted joints is a simple way to attach two structures together, and at the same time allows for a non-destructive means to separate the structures for repair or maintenance. This method of fastening has been extensively tested in the static to quasi-static regime with cross head speeds of 0.1 mm/s to 10 mm/s, but has been neglected at even higher rates of loading [Pearce, Johnson, Thomson, & Kelly, 2010]. Static testing has been extensively carried out in both bearing and tensile configuration. Within the bearing configuration the primary modes of failure are considered to be out of plane buckling and hole elongation. Both failure modes are highly dependent upon geometrical parameters of the specimen. Results for static bearing testing show a trend for increasing diameter by thickness (d/t) yields lower ultimate bearing strength. Similarly, for edge by diameter (e/d) and width by diameter w/d show an asymptotic region where failure mode abruptly changes from shear at low stress to buckling at higher stresses. This asymptotic region of failure mode alteration is common in both the geometrical parameters e/d and w/d for bearing and tensile loading configuration, and occurs at a ratio of approximately 3.0 [Kretsis & Matthews, 1985], [Matthews, Wong, & Chryssafitis, 1982]. This asymptotic behavior is has been extensively tested in the static regime where shear failure is abruptly changed to buckling for a certain e/d , w/d , and d/t ratio. The aim of this paper is to determine if any such behavior is present at high loading rates for monolithic specimens, along with subsequent determination of an optimal geometry for SHPB testing of bolted joints [Birch & Alves, 2000], [Srivastava, Shukla, & Parameswaran, 2000].

Most failures of bolted structures are predominant when loading acting on the structure is dynamic in nature thereby, motivating the need for further research on the behavior of bolted joints under impact rates of loading. In this paper a method has been developed for testing bolted

joints in a split Hopkinson pressure bar to obtain loading rates of approximately 500 MN/s. Using one dimensional wave propagation wave theory for elastic solids the following relations are established to determine loading rate, and equilibrium times [**Kolsky, 1949**].

$$F_{inc.}(t) = A_{inc.bar}E_{bar}(\varepsilon_i(t) + \varepsilon_r(t)) \quad 2.1$$

$$F_{trans.}(t) = A_{trans.bar}E_{bar}(\varepsilon(t)) \quad 2.2$$

Where $F_{inc.}$ and $F_{trans.}$ are the force on the incident and transmitted face of the SHPB. $A_{inc.bar}$ and $A_{trans.bar}$ is the cross-sectional area of the incident and transmission bars respectively. E_{bar} is the elastic modulus of the bars, and ε_i , ε_r , and ε_t are the recorded incident, reflected, and transmitted strain pulses from the adhesively bonded strain gages on the SHPB.

In order to satisfy equilibrium and buckling conditions, a set of monolithic specimens with varying length and widths were used to determine optimum geometric parameters only. Using split Hopkinson bar wave theory, specimen loading rate and equilibrium times can be calculated. This combined with visually inspecting each monolithic specimen for any mode of buckling will ensure proper specimen geometry for bolted joint testing in a SHPB setup. A finite element model had been constructed using ABAQUS 6.9-2 to mimic the behavior of the experimentally tested monolithic specimens. This model was verified to match trends of monolithic specimen loading rate, equilibrium time, and equilibrium start time for a fixed $d/t=1$, $w/d=2.83$, and varying $e/d=1,2,3,4$. Because the model was verified with experimental results, subsequently the model can be used to determine monolithic specimen behavior for other geometries that are not restrained by the diameter of the SHPB apparatus. Finally, an optimal geometry can be determined for ideal bolted joint testing where failure due to buckling and equilibrium times of specimen will be well established.

2.3 Experimental Setup of SHPB

Testing of monolithic specimens was conducted using a Split Hopkinson Pressure Bar (SHPB) apparatus. The configuration utilizes 0.75 inch 6061 Aluminum incidence and transmission bars with electro-resistive strain gages diametrically opposing centrally placed on each bar. The incident pulse was generated using a 5 inch striker powered by 30 psi of Helium. For specimen equilibrium to be obtained, and to limit dispersive effects such as Pochhammer-Cree oscillations a pulse shaping material was employed between the striker and incidence bar [**Wu & Gorham, 1997**]. Data acquisition system consists of an Ectron amplifier E513-2A with circuitry configured for half bridge and Lecroy Wave Jet 354A oscilloscope. Monolithic specimens that are geometrically similar to a uniaxial loaded bolted joint configuration were prepared with a fixed $d/t=1$, $w/d=2.83$, and varying $e/d=1, 1.5, 2, 2.5, 3, 3.5, 4, \text{ and } 4.5$ [**Riccio & Marciano,2004**]. For each e/d ratio five specimens were manufactured, and four of each was tested with one spare for any specimen that may have been lost during testing. Experimental results show 95% confidence error bars for 4 specimens. The FEM results show an average of five calculations of the same e/d configuration to reduce the bias of human calculation of takeoff and landing of incident, reflected, and transmission waves. The FEM model was constructed with ABAQUS 6.9-2 and contains an incident and transmission bar. An input pulse directly from experimental data was used for the system excitation. Using an element in the center of the incident and transmission bar within the model, the incident, reflected, and transmission waves were extracted for analysis of equilibrium times and loading rate similarly to the experiment.

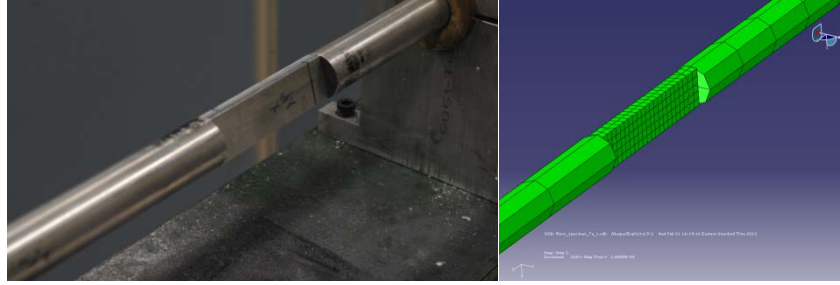


Figure 2.1 Show the ABAQUS model with specimen 7a ready to be tested on the right and the experimental setup on the left. The specimen can be seen between the incident and transmission bars.

Table 2.1 shows the geometrical parameters non-dimensionalized with respect to a hole diameter. It is important to note that the hole diameter is a fictitious value as there is no hole in the monolithic specimen. Each specimen was loaded into the SHPB setup where incidence, reflected, and transmission waves were recorded for computation of loading rate, total equilibrium time, and equilibrium start time. Parameters of w/d and e/d were fixed as the SHPB apparatus restrains from any larger specimens. Parameter geometrical definitions for monolithic specimens are illustrated in **Figure 2.2**.

Table 2.1 Geometric Parameters for experimental monolithic specimen testing

Specimen #	Monolithic Geometric Parameters							
	1a	2a	3a	4a	5a	6a	7a	8a
Fictitious Diameter (mm)	6.35	6.35	6.35	6.35	6.35	6.35	6.35	6.35
w/d	2.83	2.83	2.83	2.83	2.83	2.83	2.83	2.83
e/d	1.00	1.50	2.00	2.50	3.00	3.50	4.00	4.50
l/d	4.50	5.50	6.50	7.50	8.50	9.50	10.50	11.50
d/t	1	1	1	1	1	1	1	1
Total Width (mm)	17.96	17.96	17.96	17.96	17.96	17.96	17.96	17.96
Total Length (mm)	28.58	34.93	41.28	47.63	53.98	60.33	66.68	73.03

2.4 Results

Specimen geometries were altered according to **Table 2.1** and incident, reflected, and transmitted waves recorded for each test. Using one dimensional wave theory and **equations 2.1** and **2**, **Figures 2.3, 2.4**, and **2.5** were constructed to determine optimal specimen properties for later testing of bolted joints of similar dimensions. The force on the transmission face was calculated using **equation 2.2** where the slope of the loading pulse was used to calculate the loading rate of the specimen as shown in **Figure 2.3**. Five FEM simulations for e/d of 1, 2, 3, 4 were run using ABAQUS and averaged to smooth any outliers in the data due to the human interface between where to select where each pulse begins and ends. The general trend of the loading rate shows a slight increase from 450 MN/s to approximately 600MN/s as specimen e/d

increase. Calculation of Equilibrium times was conducted using both the force on the incident and transmission sides of the specimen. Plotting the incidence by transmission on the y-axis and time on the x-axis; equilibrium occurs when this force ratio is at unity. From this plot, the equilibrium start time of the specimen can be obtained as well as total time spent at equilibrium as shown in **Figures 2.4** and **2.5** respectively.

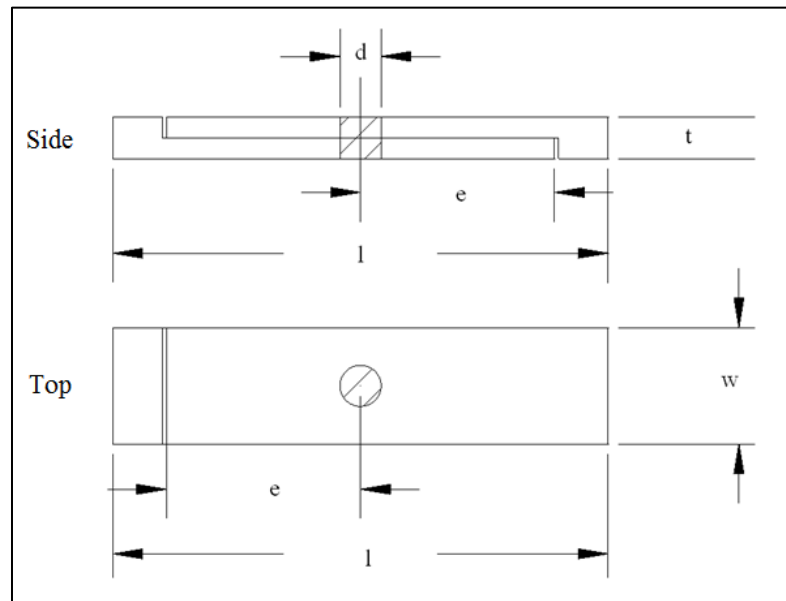


Figure 2.2 Geometrical definitions for monolithic specimen size descriptions

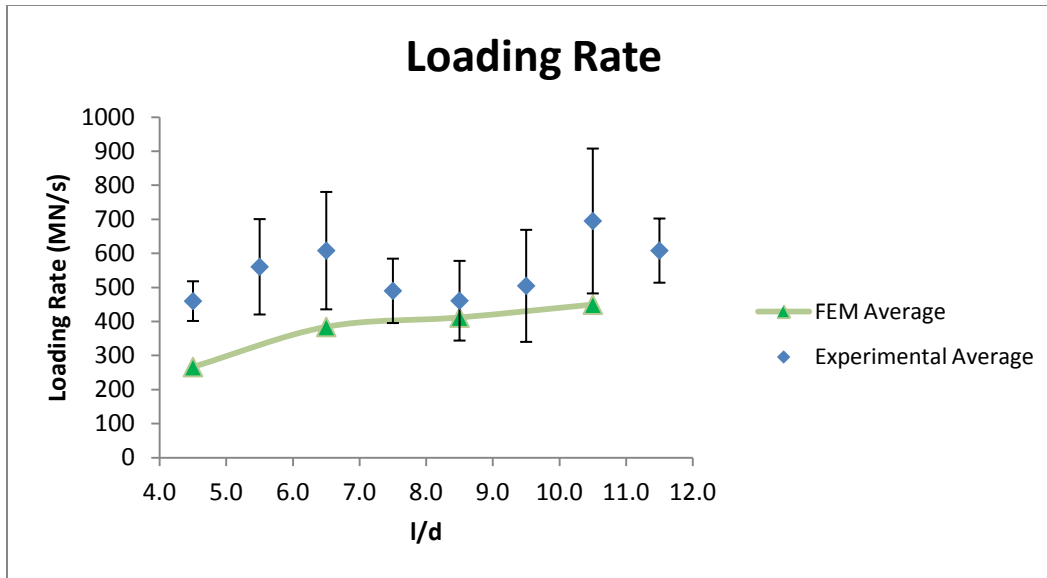


Figure 2.3 Loading rate from transmitted force of specimen for varying e/d in compression.

Experimental error bars are calculated with 95% confidence interval

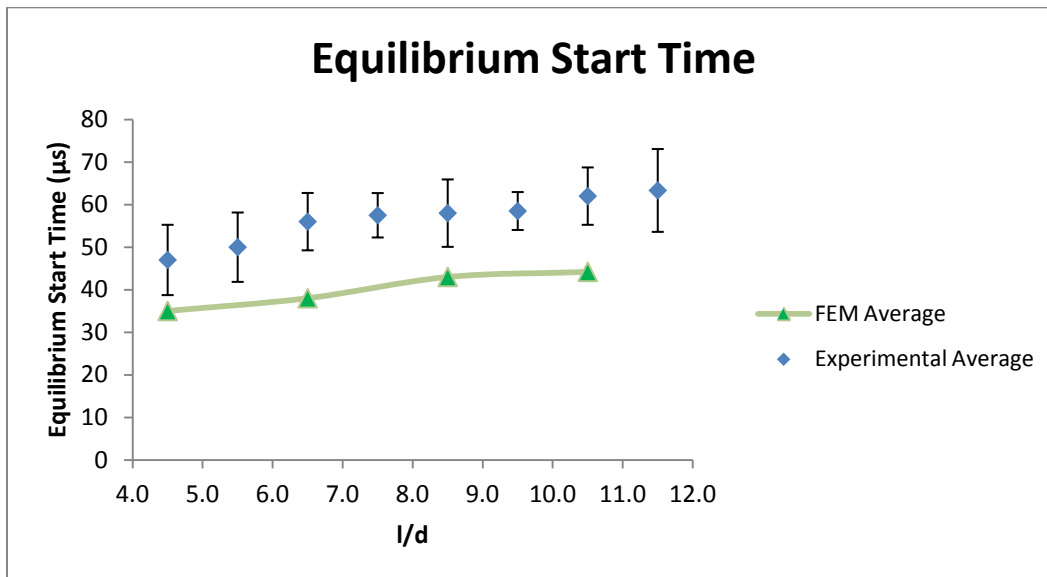


Figure 2.4 The amount of time it takes the specimen to first reach equilibrium for varying e/d in compression. Experimental error bars are calculated with 95% confidence interval

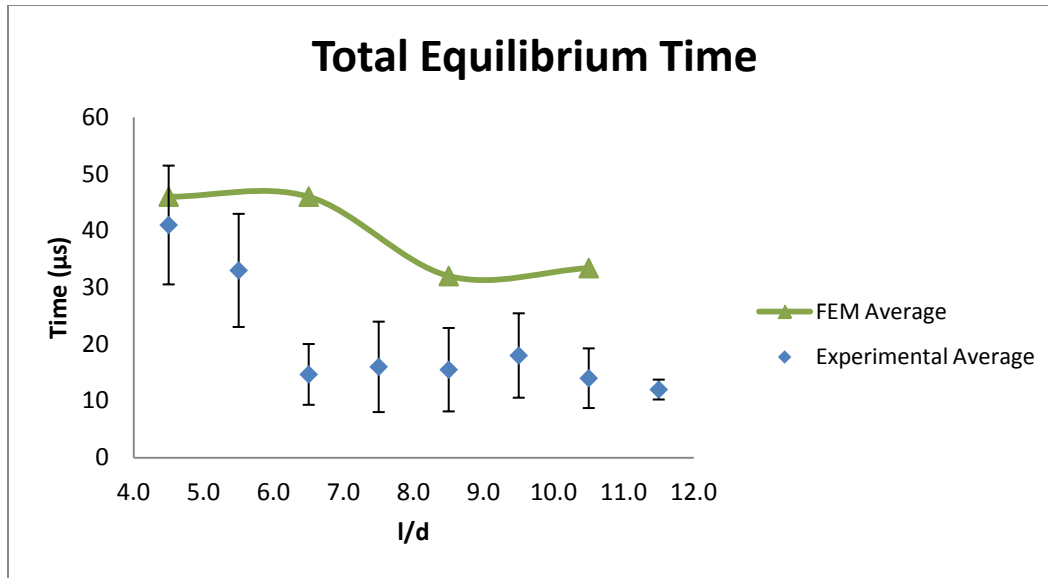


Figure 2.5 Total amount of time the specimen is at equilibrium for varying e/d in compression.

Experimental error bars are calculated with 95% confidence interval

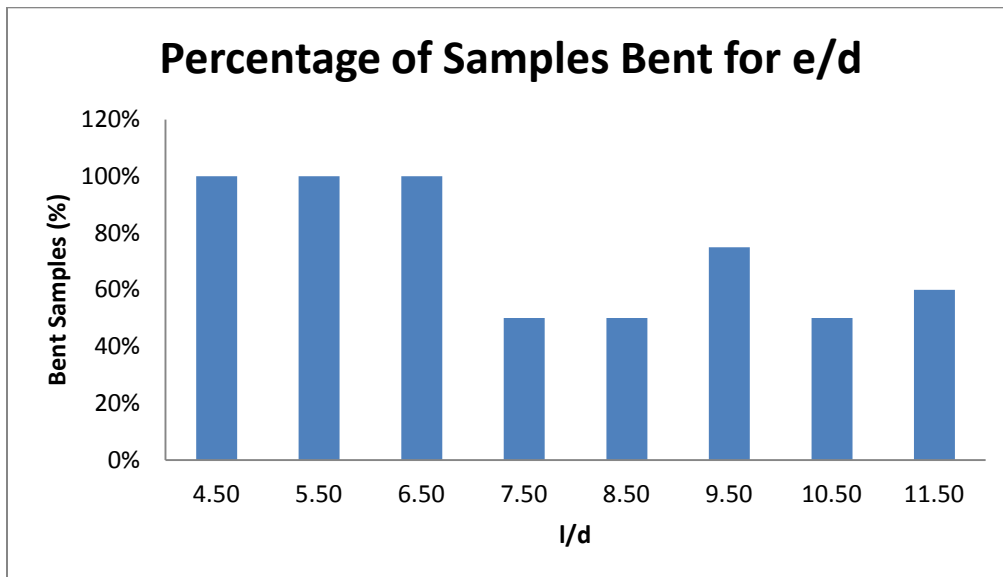


Figure 2.6 Samples that have been bent due to testing. All samples were visually inspected against a flat surface to determine if permanent deformation due to bending has occurred

Using the FEM model that was validated with experimental results, a study was conducted where parameters of monolithic specimen geometry w/d , d/t , and l/d were varied using 48 different specimens as shown in **Table 2.1**.

Table 2.2 Geometric Parameters for Finite Element monolithic specimen testing

Specimen #	FEM Runs							
	w/d	dimensions w (mm)	l/d	dimensions l (mm)	d/t	dimensions t (mm)	e/d	dimensions e (mm)
1	1	6.35	5.5	34.93	1	6.35	1.5	9.53
2	2	12.70	5.5	34.93	1	6.35	1.5	9.53
3	3	19.05	5.5	34.93	1	6.35	1.5	9.53
4	4	25.40	5.5	34.93	1	6.35	1.5	9.53
5	5	31.75	5.5	34.93	1	6.35	1.5	9.53
6	6	38.10	5.5	34.93	1	6.35	1.5	9.53
7	1	6.35	7.5	47.63	1	6.35	2.5	15.88
8	2	12.70	7.5	47.63	1	6.35	2.5	15.88
9	3	19.05	7.5	47.63	1	6.35	2.5	15.88
10	4	25.40	7.5	47.63	1	6.35	2.5	15.88
11	5	31.75	7.5	47.63	1	6.35	2.5	15.88
12	6	38.10	7.5	47.63	1	6.35	2.5	15.88
13	1	6.35	9.5	60.33	1	6.35	3.5	22.23
14	2	12.70	9.5	60.33	1	6.35	3.5	22.23
15	3	19.05	9.5	60.33	1	6.35	3.5	22.23
16	4	25.40	9.5	60.33	1	6.35	3.5	22.23
17	5	31.75	9.5	60.33	1	6.35	3.5	22.23
18	6	38.10	9.5	60.33	1	6.35	3.5	22.23
19	1	6.35	11.5	73.03	1	6.35	4.5	28.58
20	2	12.70	11.5	73.03	1	6.35	4.5	28.58
21	3	19.05	11.5	73.03	1	6.35	4.5	28.58
22	4	25.40	11.5	73.03	1	6.35	4.5	28.58
23	5	31.75	11.5	73.03	1	6.35	4.5	28.58
24	6	38.10	11.5	73.03	1	6.35	4.5	28.58
25	1	6.35	5.5	34.93	0.5	12.7	1.5	9.53
26	2	12.70	5.5	34.93	0.5	12.7	1.5	9.53
27	3	19.05	5.5	34.93	0.5	12.7	1.5	9.53
28	4	25.40	5.5	34.93	0.5	12.7	1.5	9.53
29	5	31.75	5.5	34.93	0.5	12.7	1.5	9.53
30	6	38.10	5.5	34.93	0.5	12.7	1.5	9.53
31	1	6.35	7.5	47.63	0.5	12.7	2.5	15.88
32	2	12.70	7.5	47.63	0.5	12.7	2.5	15.88
33	3	19.05	7.5	47.63	0.5	12.7	2.5	15.88
34	4	25.40	7.5	47.63	0.5	12.7	2.5	15.88
35	5	31.75	7.5	47.63	0.5	12.7	2.5	15.88
36	6	38.10	7.5	47.63	0.5	12.7	2.5	15.88
37	1	6.35	9.5	60.33	0.5	12.7	3.5	22.23
38	2	12.70	9.5	60.33	0.5	12.7	3.5	22.23
39	3	19.05	9.5	60.33	0.5	12.7	3.5	22.23
40	4	25.40	9.5	60.33	0.5	12.7	3.5	22.23
41	5	31.75	9.5	60.33	0.5	12.7	3.5	22.23
42	6	38.10	9.5	60.33	0.5	12.7	3.5	22.23
43	1	6.35	11.5	73.03	0.5	12.7	4.5	28.58
44	2	12.70	11.5	73.03	0.5	12.7	4.5	28.58
45	3	19.05	11.5	73.03	0.5	12.7	4.5	28.58
46	4	25.40	11.5	73.03	0.5	12.7	4.5	28.58
47	5	31.75	11.5	73.03	0.5	12.7	4.5	28.58
48	6	38.10	11.5	73.03	0.5	12.7	4.5	28.58

The geometries selected were tested in the ABAQUS model constructed for the experimental validation, however for study in **Table 2.1** larger diameter bars were needed to accommodate the larger specimens. For Hopkinson bar experiment an equation may be needed to correct for the additional axial stress developed due to radial inertia, however radial inertia was neglected because the materials tested have high flow stresses, unlike soft materials like rubber or gels [Warren & Forrestal, 2009]. With the model constructed, trends for loading rate, equilibrium start time, and total equilibrium time are shown in proceeding figures.

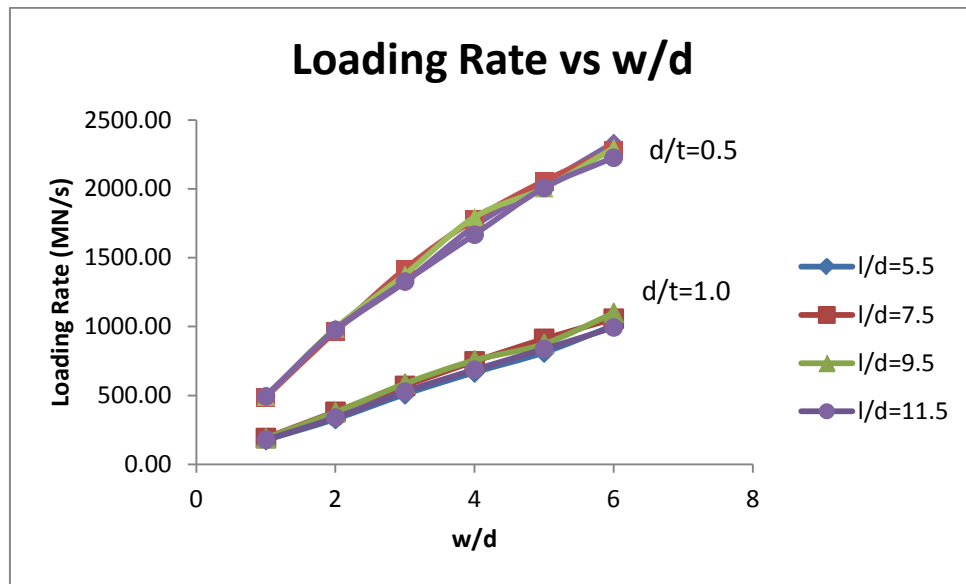


Figure 2.7 Loading rate in MN/s for varying l/d , w/d , and $d/t=1.0$ and 0.5

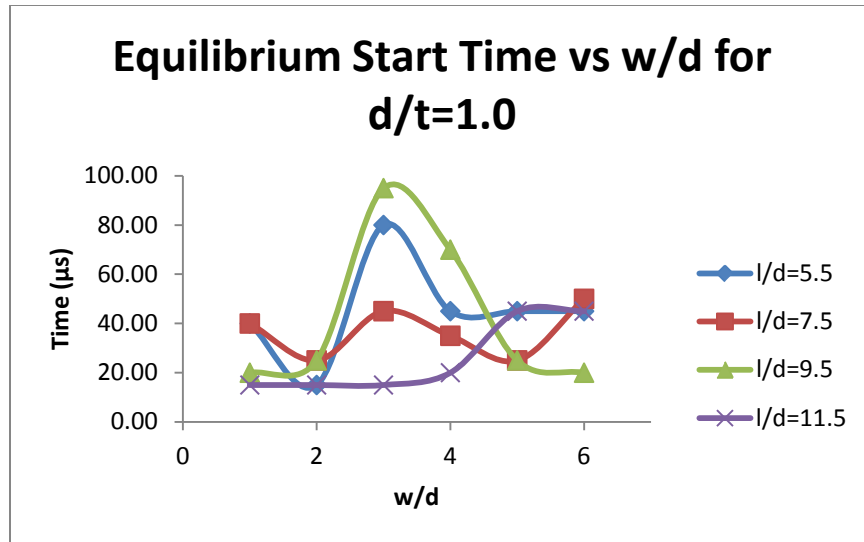


Figure 2.8 Specimen equilibrium start time for varying l/d, w/d, and d/t=1.0

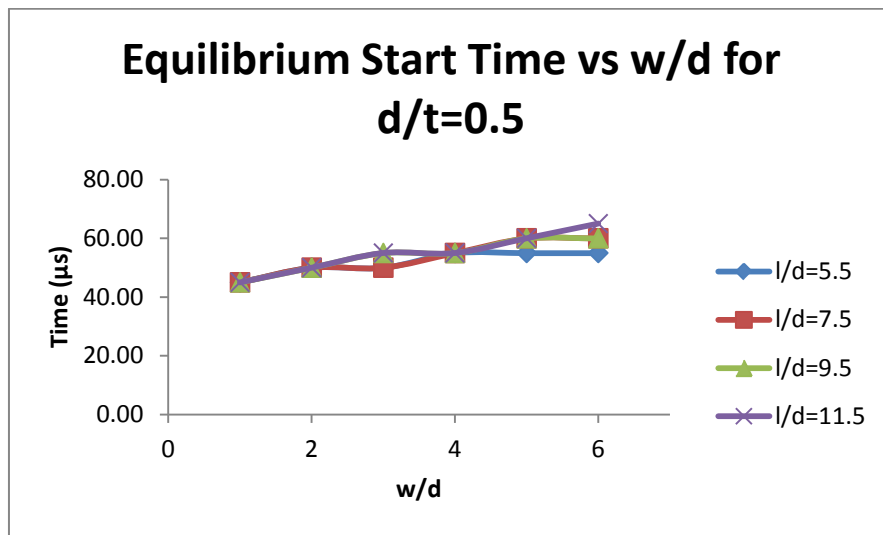


Figure 2.9 Specimen equilibrium start time for varying l/d, w/d, and d/t=0.5

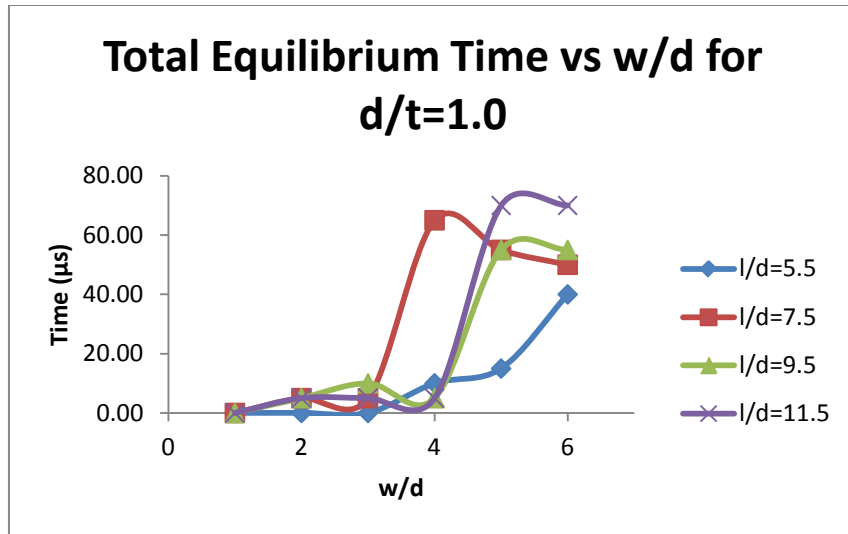


Figure 2.10 Specimen total time spent at equilibrium during loading for varying l/d, w/d, and d/t=1.0

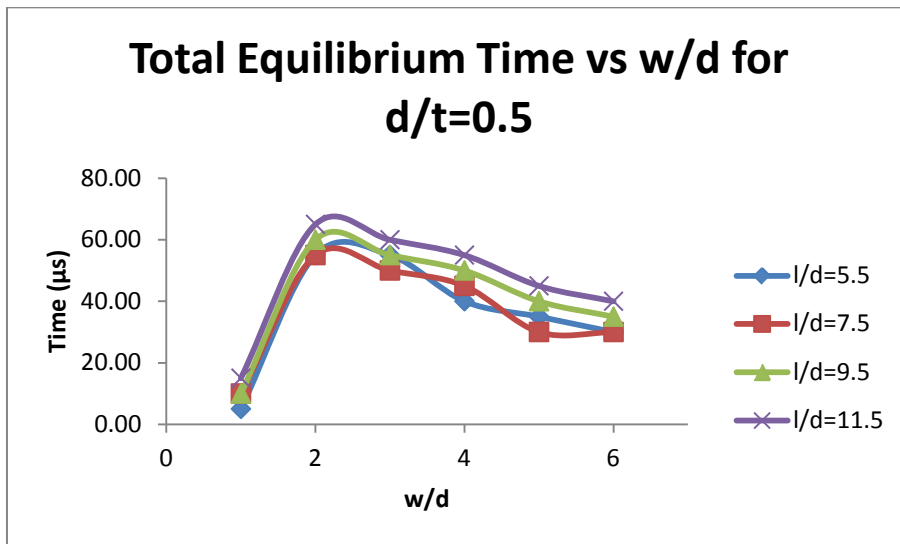


Figure 11 Specimen total time spent at equilibrium during loading for varying l/d, w/d, and d/t=0.5

2.5 Discussion

Ideal specimen properties are high total equilibrium times, low equilibrium start times and low chances of buckling or bending. In the literature, it can be seen that equilibrium typically occurs at approximately $17\mu\text{s}$ to $20\mu\text{s}$ for sample lengths of 0.76mm to 1.5mm in length respectively. Length of the tested monolithic specimens varied from 1.125in - 2.875in (73.025mm). For range of specimen length, it can be seen that the equilibrium start time is much higher, ranging from $45\mu\text{s}$ to $63\mu\text{s}$ due to inertia and non-uniform deformation due to wave propagation effects [Wu & Gorham, 1997]. The increase in equilibrium start time is dependent on the length of the specimen, as the longer specimen requires more time for the pulse to propagate. A finite incidence pulse is generated, tradeoff occurs between total time spent in equilibrium and equilibrium start times. This effect can be noticeably seen at e/d ratio of approximately 2.5. This behavior reflects nicely shown in **Figure 2.6** with the amount of specimens recorded as bent decreases with a decrease in total time spent in equilibrium. The FEM results follow closely to the actual experimental results in that general trends are still kept precise. However the accuracy of the model shows that some assumptions made in the model need to be refined. Error is introduced between the interface between the specimen, incidence, and transmission bars has been modeled to be in perfect slip contact. This can cause the model to underestimate the actual equilibrium start time and over estimate the total time spent at equilibrium.

The ABAQUS model used in the study for all geometries listed in **Table 2** show interesting trends for loading rates, equilibrium start times, and total equilibrium time. **Figure 2.7** show increasing w/d will yield a linear increase in loading rate for the specimen irrespective of varying l/d . Increasing the thickness of the specimen by a factor of two yields a similar result only magnitudes of loading rate are slightly more than doubled. This behavior mimics the theory of

impedance. Where, increasing w/d will eventually converge at unity, rendering a perfect junction interface where the loading rate would match the incident pulse, as the cross sectional area of the specimen approaches the cross sectional area of the incident bar. **Figures 2.8 and 2.9** show equilibrium start times for varying l/d , and w/d for both cases of $d/t=1.0$ and $d/t=0.5$. **Figure 2.8** shows a general trend of sporadic behavior with maximum equilibrium times at $e/d \approx 3.0$. However, the equilibrium start times do appear to increase with increasing w/d . **Figure 2.9** equilibrium start times were simulated for $d/t = 0.5$. This figure shows a linear increase in equilibrium start time for increasing w/d and is not affected by varying l/d . **Figures 2.10 and 2.11** shows the total amount of time the specimen spends in equilibrium. **Figure 2.10** shows a great increase in total equilibrium time for a w/d of approximately 4 to 4.5. Similarly, for **figure 2.12** a sudden jump in equilibrium start time can be seen at $w/d=2$. Both **figures 2.10 and 2.11** agree that increasing l/d increases the total amount of time the specimen is at equilibrium.

2.6 Recommendations and Conclusion

From the collected data it can be deduced that there does exist an optimum bolted joint geometry that can reach equilibrium and avoid local bending. **Figures 2.3, 2.4, 2.5, 2.6** shows that increasing a specimen length will decrease the chance of buckling or local bending to occur, at the same time there exists a geometry where minimal local bending takes place with relatively high equilibrium times. The ideal bolted joint parameters that would yield the best result for a 19.05 mm diameter Hopkinson bar would be $e/d=2.5$ or total length of 47.63 mm for minimal local bending and maximum time spent at equilibrium for a dynamic loading rate of approximately 500 MN/s. Using the model constructed it is possible to vary in w/d , l/d , and d/t with a larger bar diameter for testing of larger specimens. For optimum results to be obtained during testing of bolted joint it is recommended for $d/t=1.0$, geometries of $w/d > 4.0$ and $l/d=5.5$

thru 11.5 will yield best results. Similarly, for optimum results to be obtained it is recommended for $d/t=0.5$, geometries of $2.0 < w/d < 4.0$ and $l/d=5.5$ thru 11.5 will yield best results.

2.7 References

- Birch, R., & Alves, M. (2000). Dynamic Failure of Structural Joint Systems. *Thin-Walled Structures*, 137-154.
- Pearce, G. M., Johnson, A. F., Thomson, R., & Kelly, D. W. (2010). Experimental Investigation of Dynamically Loaded Bolted Joints in Carbon Fibre Composite Structures. *Appl Compos Mater*, 271-291.
- Kretsis, G., & Matthews, F. (1985). The Strength of Bolted Joints in Glass Fibre/ Epoxy Laminates. *Composites*, Volume 16. No 2.
- Kolsky, H. (1949). An Investigation of the Mechanical Properties of Materials at very High Rates of Loading. *Proc. Phys. Soc.*, 676-700.
- Riccio, A., & Marciano, L. (2004). Effects of Geometrical and Material Features on Damage Onset and Propagation in Single-lap Bolted Composite Joints under Tensile Load: Part 1 - Experimental Studies. *Composite Materials*, 2071-2090.
- Smith, P., Pascoe, K., Polak, C., & Stroud, D. (1986). The Behaviour of Single-Lap Bolted Joints in CFRP Laminates. *Composite Structures*, 41-55.
- Srivastava, V., Shukla, A., & Parameswaran, V. (2000). Experimental Evaluation of the Dynamic Shear Strength of Adhesive-Bonded Lap Joints. *Journal of Testing and Evaluation*, 438-442.
- Warren, T., & Forrestal, M. (2009). Comments on the Effect of Radial Inertia in the Kolsky Bar Test for an Incompressible Material. *Experimental Mechanics*, 1253-1255.
- Wu, X., & Gorham, D. (1997). Stress Equilibrium in the Split Hopkinson Pressure Bar Test. *J. Phys*, C391-C396.

Chapter 3 Evaluating Bolted Joint Behavior at High Strain Rates

3.1 Abstract

Bolting two members together in a structure serves as an easy and non-destructive method of joining materials which finds prominent usage in automotive, aeronautical and industrial applications. Extensive literature exists characterizing the failure of bolted joints under quasi-static rates of loading. However, crashworthiness characteristics of a bolted joint in a structure are widely unknown and needs further investigation. In our current investigation, an attempt has been made to observe response of bolted joints under impact rates of loading using a split Hopkinson pressure bar (SHPB). The current article addresses bearing failure characteristics of bolted joints, under impact loading, which has been restricted to joint slip. A relationship between loading rate, bolt pre-load and maximum transmitted force before joint slip has been observed as well. This would in-turn provide us beneficial information on subsequent design of bolted joints where behavior under impact loading is of main concern.

Keywords: Bolted joint, Split Hopkinson Pressure Bar, Bearing stress

3.2 Introduction to Bolted Joints

Bolted joints are extensively used in many automotive and aeronautical sectors where two members are bolted together. This particular method of fastening is vastly used in many industrial disciplines as it serves as an easy and non-destructive method to join and subsequently disassemble a complex structure. This directly implicates the necessity to investigate how the geometrical mechanisms of bolted joints are affected when subjected to a variety of loading rates. Extensive quasi-static testing has been conducted to characterize bolted joint failure for a myriad of different geometrical configurations. Including monitoring the clamp-up pressure caused by torquing a nut on the bolt during testing with different sized washers. [Yan et al.,

1999]. Similarly, [Wang et al., 1996] investigated bolt pre-load as it was monitored during compression testing of composite bolted joints. It was observed that the bolt pre-load varies with applied force and can be used to detect bearing damage. With quasi-static rates of loading, bolted joints have been tested with a myriad of different materials and geometries. Low rates of loading in compression show that there exists an asymptotic region where failure modes abruptly change. This asymptotic region of failure mode alteration is shown to exist by varying joint geometrical parameters. This behavior is common for both bearing and tensile loading configurations, and in [Kretsis & Matthews, 1985; Smith et al., 1986] has been experimentally determined to occur at a w/d or e/d value of approximately 3.0. Typically, bolted joint parameters e , w , and t are non-dimensionalized with respect to the bolt diameter d . Where e/d , w/d , and d/t ratios denote the edge distance from hole center to specimen edge, width, and thickness of the joining members respectively.

However, minimal literature exists describing the behavior of bolted joints under time-dependent loading conditions. It has been shown that there exists a range of optimum geometries where localized bending of the joint can be avoided and equilibrium attained for long specimens under compressive loading conditions using a Split Hopkinson Pressure Bar (SHPB) [Tekalur et al., 2012]. Under dynamic compression, the width w , length l , thickness t , and diameter d are the dominant geometrical parameters associated with a bolted joint. These geometrical parameters are typically non-dimensionalized with respect to the diameter of hole (cut into the material under investigation) yielding the parameters e/d , w/d and t/d .

In our current investigation, an attempt has been made to observe response of bolted joints under impact rates of loading using a SHPB. The current article addresses how bearing failure characteristics of bolted joints under impact loading are dominated by joint slip with the used

geometry and material. Joint slip can be defined as the relative movement of the joint members. This is caused by surpassing the static friction force with an impact load, causing subsequent slip between the joined members. Slip occurs as there is an average of 4 thousandths of an inch of hole clearance between the bolt and hole. This is a typical industry standard for loose fit bolts. Compressive force on the specimen and bolt pre-load on the joint will be monitored in real time, yielding how this effect the bearing strength of the joint as it is under a time dependent uniaxial load. A relationship between loading rate, bolt pre-load and maximum force transmitted before joint slip has been observed. This investigation show there exist strong dependence on compressive joint strength with loading rate.

3.3 Materials and Methods

The schematic of the experimental set-up is shown in **Figure 3.1**. The SHPB comprises of an incident and an identical transmission bar made of 6061 T6 Aluminum 6 feet in length and 0.75 inch in diameter. A striker is fired from a Helium powered gas gun which produces a compressive pulse in the incident bar. Pulse shapers are used to reduce the signal noise in the incident pulse and to assist in attaining force equilibrium within the specimen during the test by elongating the pulse width. The responses are read by the strain gages bonded on the incident and transmission bar with Vishay AE-10 epoxy. The gages are placed diametrically opposed and wired in a half bridge configuration to cancel bending and to amplify axial strain. Data acquisition is carried out by an Ectron amplifier (Model513-2A) and a LeCroy digital oscilloscope (Model354A). High speed images of the bolted joint under impact load were captured with a phantom camera model V12.0 set to a frame rate of 110,000 fps. A single shear lap joint of two aluminum links was tested at varying geometries. The geometries were selected to accommodate within a SHPB apparatus.

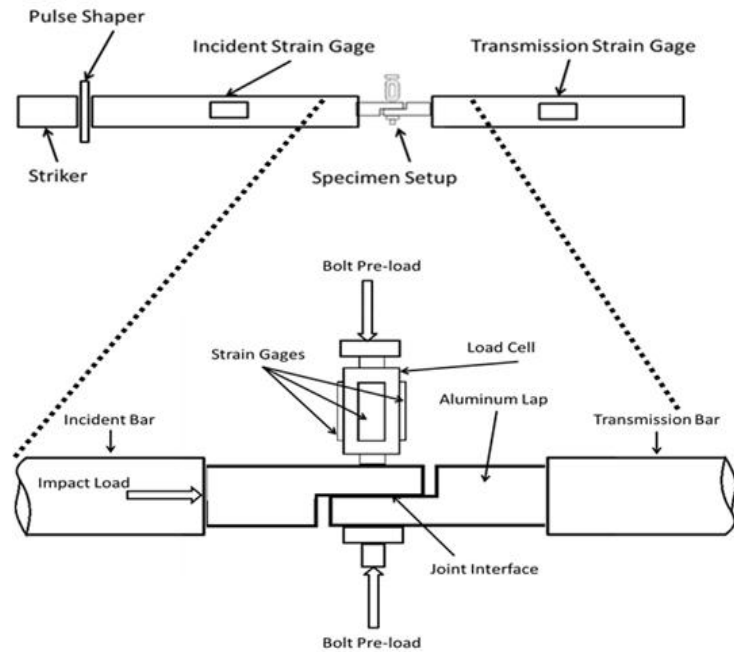


Figure 3.1 Schematic of the SHPB apparatus used in current investigation. Zoomed in view of specimen region shows the placement of the load cell to monitor bolt pre-load.

For select geometries the aluminum bolted joint is outfitted with a load cell to measure the preload of the joint created from torquing the nut on the bolt. **Figure 3.2** shows the corresponding calibration curves. This load cell has four strain gages wired in a full Wheatstone bridge configuration to amplify the axial load measured from the bolt. Because of the complex shape of the load cell, the axial force is difficult to attain from the taken strain measurements. In order to test the linearity, as a verification method, the load cell was calibrated against a MTS machine (10kN load cell) to build a calibration curve of the strain measured to the force exerted. This calibrated load cell is used to monitor the bolt pre-load during the impact test to determine how preload of a bolt is affected during the event.

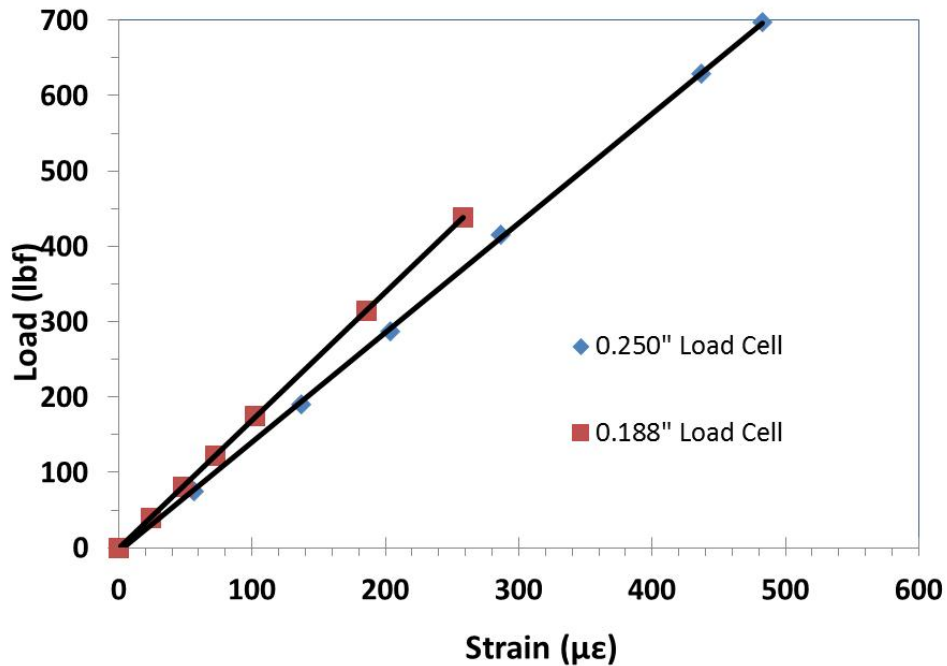


Figure 3.2 Load cell calibration for bolt diameters of 0.25\" and 0.188\".

Using a set of geometries recommended for bolted joint testing, adopted from [Tekalur et al. 2012], 4 different specimen identifications were created as listed in Table 3.1. This includes l/d ratios of 7.5 and 11.5, w/d ratios of 4.0 and 3.0, e/d ratios of 2.5 and 4.5, and d/t ratios of 0.5 and 1.0 for a total of 20 tests. These geometries were tested with pre-loads measuring at 0lbf, 100lbf, 300lbf, 500lbf, and 700lbf. The pre-loads were selected with values that were within the range of the compressive yield strength of the Al 6061 T6 material.

Table 3.1 Specimen geometry and set preload for specimens tested in uniaxial compression in the SHPB.

Specimen ID	e/d	w/d	l/d	d/t	Preload (lbf)
1	2.5	4	7.5	1	0
1	2.5	4	7.5	1	100
1	2.5	4	7.5	1	300
1	2.5	4	7.5	1	500
1	2.5	4	7.5	1	700
2	4.5	4	11.5	1	0
2	4.5	4	11.5	1	100
2	4.5	4	11.5	1	300
2	4.5	4	11.5	1	500
2	4.5	4	11.5	1	700
3	2.5	3	7.5	0.5	0
3	2.5	3	7.5	0.5	100
3	2.5	3	7.5	0.5	300
3	2.5	3	7.5	0.5	500
3	2.5	3	7.5	0.5	700
4	4.5	3	11.5	0.5	0
4	4.5	3	11.5	0.5	100
4	4.5	3	11.5	0.5	300
4	4.5	3	11.5	0.5	500
4	4.5	3	11.5	0.5	700

3.4 Results and Discussion

A time dependent load is imparted by SHPB on the bolted joint. The loading rate and equilibrium state are established in accordance with the wave theory [Kolsky, 1949].

$$F_{inc.}(t) = A_{inc.bar}E_{bar}(\varepsilon_i(t) + \varepsilon_r(t)) \quad 3.1$$

$$F_{trans.}(t) = A_{trans.bar}E_{bar}(\varepsilon(t)) \quad 3.2$$

$$\sigma_{bearing, max} = \frac{F_{trans,max}}{A_{bearing}} \quad 3.3$$

Where, $F_{inc.}$ and $F_{trans.}$ are the forces on the incidence and transmission face of the SHPB. $A_{inc.bar}$ and $A_{trans.bar}$ denote the cross-sectional area of the incident and transmission bars respectively. E_{bar} indicates the elastic modulus of the bars, and ε_i , ε_r , and ε_t represent the recorded incident, reflected, and transmitted pulses. Subsequently, the maximum bearing stress is calculated from the maxing transmitted force by the cross-sectional bearing area, as represented by **equation 3.3**. **Figure 3.3** shows a typical plot of pulses obtained in a SHPB during testing of bolted joints. The duration and amplitude of the incident pulse are 140 μ s and 1140 μ ε respectively.

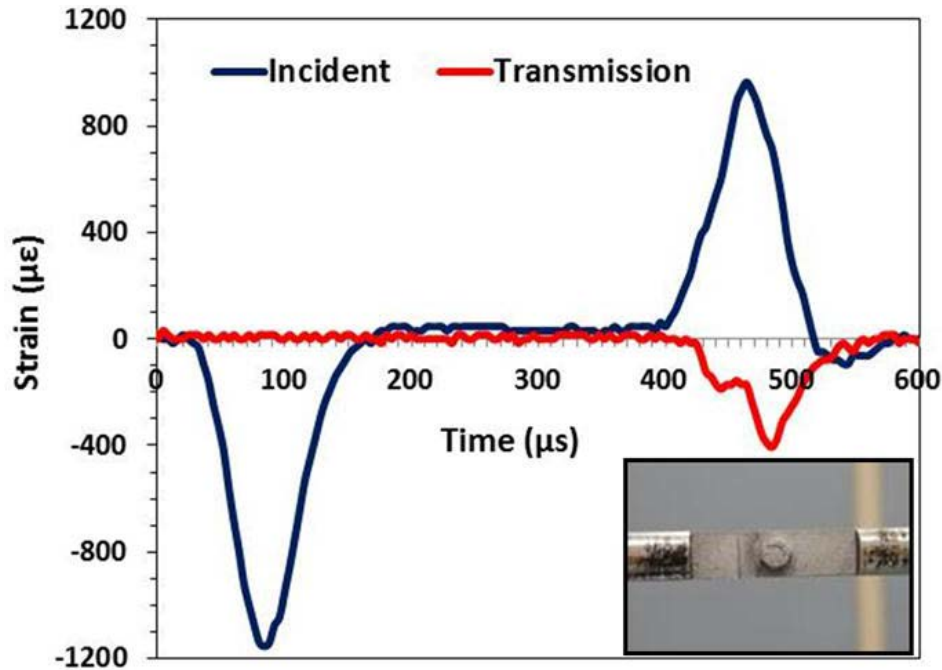


Figure 3.3 Plot of pulses obtained in incident and transmission bars. Shown in the lower right is the bolted joint sandwiched within the SHPB incident and transmission bars.

3.5 Effect of slip

It is desired that the ratio of incident to transmission force converges to one during equilibrium. However, due to the length, complex geometry, and material mismatch with the bolt, equilibrium is not easily attained; similar observations were documented with monolithic specimens with uniform geometry and small length [Tekalur et al., 2012]. With the bolted joints it is hypothesized that the sudden deviation from the equilibrium during testing can be attributed to joint slip which has been confirmed from the high speed images as shown in **Figure 3.4**. The image capture times were in direct correlation with the initiation of incident pulse.

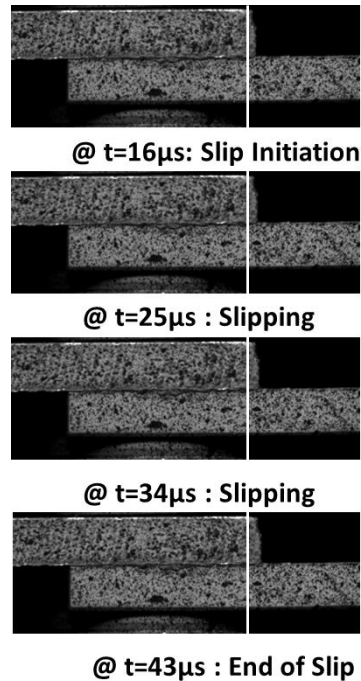


Figure 3.4 High speed images of bolted joint slipping. Scale bar represents 0.125 inches and white reference line correlates to slip initiation at 16 μ s.

With reference to **Figure 3.3**, the transmission strain time curve shows the joint slip region starting at approximately 832 μ s until 859 μ s. Four distinct regions of specimen loading can be similarly observed from the plot of transmitted force versus time: (a) initial loading, (b) joint slip, (c) post joint slip loading, and (d) unloading, as shown in **Figure 3.5**. After initial loading ramp, we have a region of slip where coulomb friction force stays constant until bolt hole clearance is eliminated. Post joint slip, loading is once again imparted on the joint with the remaining incident pulse and equilibrium is subsequently attained until unloading phase of the pulse occurs. This is verified with the captured high speed images. As it can be seen from **Figure 3.4**, slip in the members of the single lap joint occurs relative to one another commencing after 16 μ s from the start of incident pulse. The members begin to slip, and equilibrium starts degrading. As shown with the reference (white) line the top member slides until the bolt hole

clearance is eliminated and the post slip joint loading rate is again resumed starting at $43\mu\text{s}$ and equilibrium re-established.

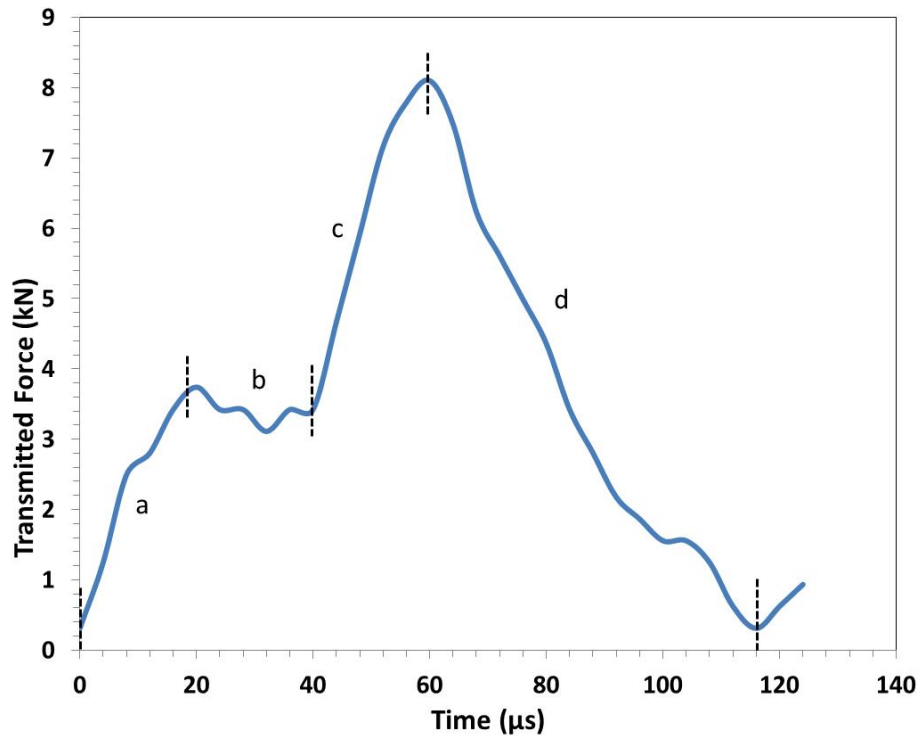


Figure 3.5 Plot of transmitted force versus time: (a) initial loading, (b) joint slip, (c) post joint slip loading, and (d) unloading.

The force measured on the transmission side of the specimen before slip can be attributed to coulomb static friction force, and similarly during slip, kinetic friction force until the bolt comes into contact with both members and the second loading rate is initiated. Based on the dynamics of dry friction, it has been observed that as relative velocity between two surfaces increases, the kinetic coefficient of friction also increases [Elmer, 1997]. This behavior can be similarly extended to a bolted joint under a variety of loading rates. As it can be seen from **Figure 3.6**, a linear behavior exists between specimens tested at higher loading rates and a relative increase in transmitted force during joint slip.

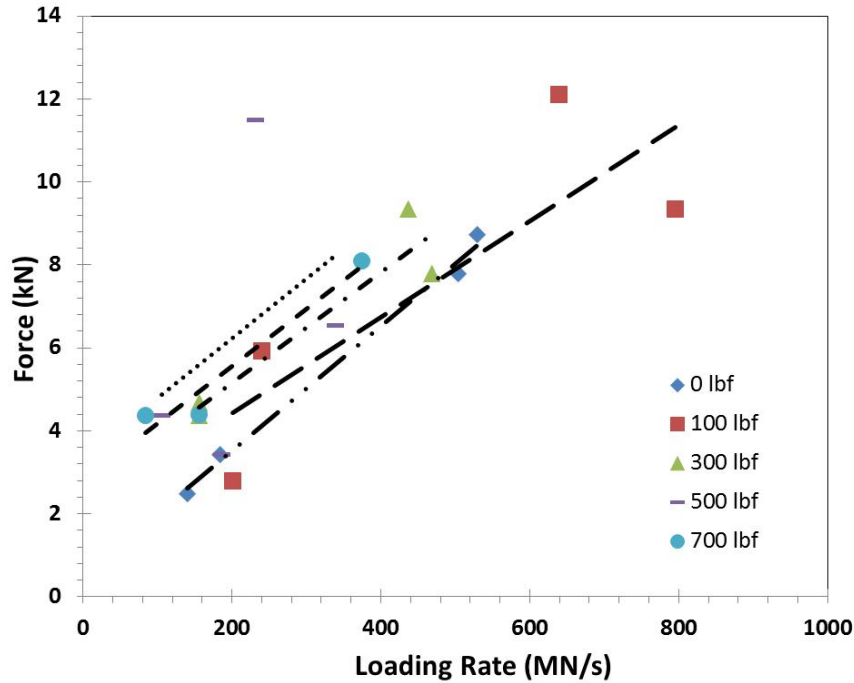


Figure 3.6 Loading rate vs. Force transmitted of specimen during slip for varying pre-loads.

3.6 Effect of joint pre-load

Figure 3.7 represents a plot of the maximum bearing stress in the bolted joint against joint pre-load for different specimen. As it can be seen from **Figure 3.7**, maximum bearing stress is independent of joint pre-load but dependent upon joint geometry. Complementing the bearing stress is **Figure 3.8** where the loading rate is plotted versus the joint pre-load. Once again, overall experimental trends show that at a pre-load of 100 lbf the loading rate is maximum for all geometries tested; however, subsequent higher pre-loads become independent of loading rate.

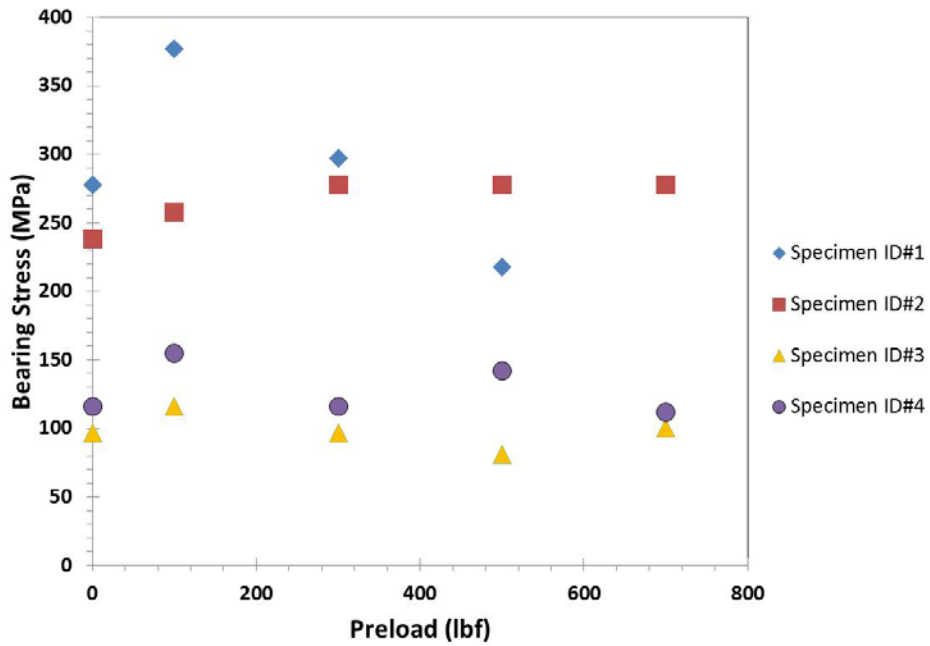


Figure 3.7 Plot of maximum bearing stress versus pre-load of bolt for varying geometries where specimen ID# represent the geometrical parameters as listed in **Table 1**.

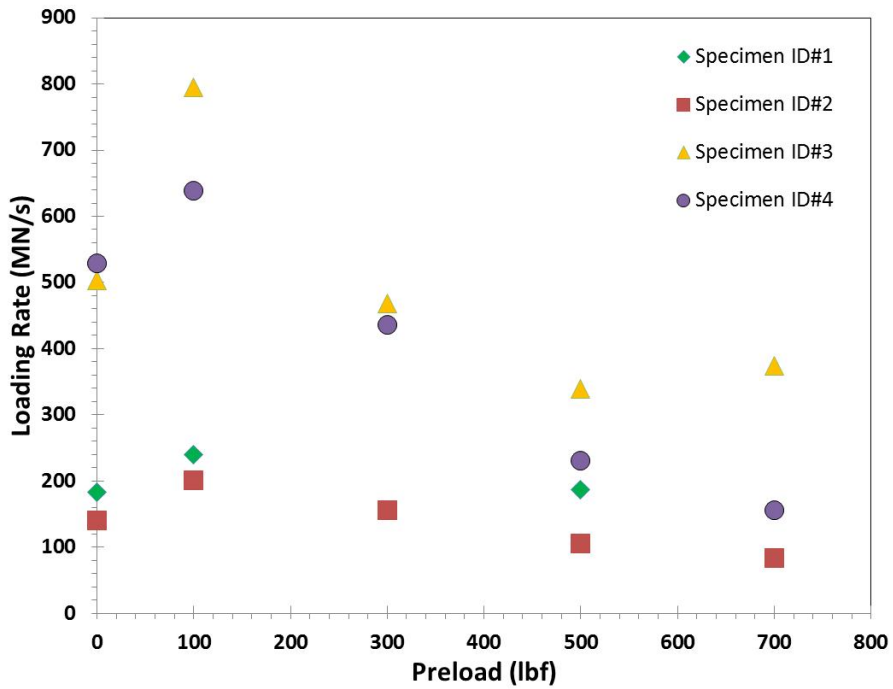


Figure 3.8 Plot of loading rate versus pre-load of bolt for varying geometries where specimen ID# represent the geometrical parameters as listed in **Table 1**.

Figure 3.9 shows the strain-time history of the load cell mounted on the specimen during testing. For the purposes of clarity, the curves for the 100lbf, 300lbf, and 500lbf have been eliminated. A monolithic sample comprising of a single piece of aluminum was machined to the same geometry as a bolted joint specimen with a load cell mounted between the bolt head and specimen surface. This monolithic sample was tested with the other specimens to provide a baseline signal that represents an ideal bolted joint and load cell configuration. The strain signal obtained for the monolithic load cell is quite noticeably not zero as transverse wave propagation provides a major contribution to the signal. Overall, the plot shows that increased preload on the joint yield a smaller deviation in strain during loading, and even seems to converge to the monolithic ideal bolted joint scenario for high pre-loads. Each of the pre-loads show a compression loading type on the load cell meaning a tensile reactive force in the bolt. In **Figure 3.9** for all pre-loads the initial peak of load during impact is simply superposed to the pre-load of the bolt. This additional load on the bolt diminishes for greater pre-loads as seen for the 700lbf pre-load in magnitude comparison to the monolithic cell.

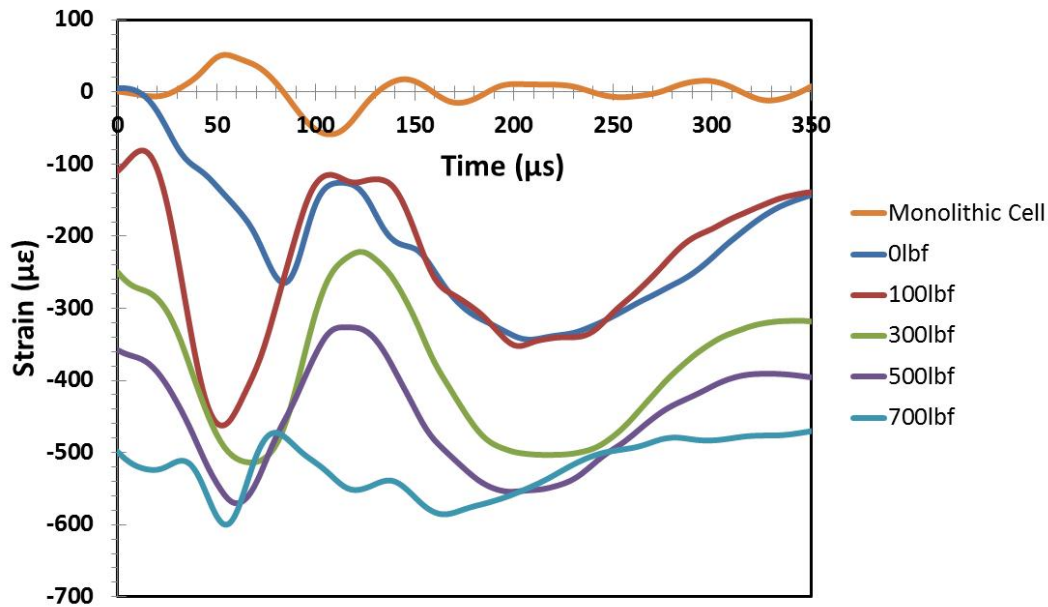


Figure 3.9 Strain time curves from the 0.25" load cell at pre-loads of 0lbf, 100lbf, 300lbf, 500lbf, 700lbf, and monolithic base test.

4. Conclusion

Bearing failure characteristics of bolted joints studied in this investigation have restricted to joint slip. Relative joint slip caused by a time dependent load has been experimentally shown that joint kinetic friction forces are directly related to the loading rate imparted upon the joint. In that as loading rate increases the static friction force increases with linear behavior. In addition bolt pre-load was monitored to determine that impact rates of loading in a shearing direction can greatly supplement the pre-load strain experienced in the bolt.

3.8 References

- Bickley, W. (1928). The Distribution of Stress Round a Circular Hole in a Plate. *Royal Soc.* , 383-415.
- Bouchard, B., Hall, B., Restivo, G., & Cloud, G. (2010). Novel Insert Design for Thick Single Lap Bolted Composite Joints. *SEM Annual Conference* (pp. 405-412). Indianapolis: Society of Experimental Mechanics Inc.
- Chen, W., & Song, D. F. (2003). Dynamic Small Strain Measurements of a Metal Specimen with a Split Hopkinson Pressure Bar. *Society of Experimental Mechanics*, 20-23.
- Elmer, F.-J. (1997). Nonlinear Dynamics of Dry Friction. *J. Phys. A: Math. Gen.*, 6057-6063.
- Herrera-Franco, P. J., & Cloud, G. L. (1992). Strain-Relief Inserts for Composite Fasteners-An Experimental Study. *Composite Materials*, 751-768.
- Jong, T. D. (1977). Stresses Around Pin Loaded Holes in Elastically Orthotropic or Isotropic Plates. *Composite Materials*, 313-331.
- Kolsky, H. (1949). An Investigation of the Mechanical Properties of Materials at very High Rates of Loading. *Proc. Phys. Soc.*, 676-700.
- Kretsis, G., & Matthews, F. (1985). The Strength of Bolted Joints in Glass Fibre/ Epoxy Laminates. *Composites*, Volume 16. No 2.
- Restivo, G., Isaicu, G. A., & Cloud, G. L. (2008). Low-Cost Non-Destructive Inspection by Simplified Digital Speckle Interferometry. *J Nondestruct Eval*, 135-142.
- Smith, P., Pascoe, K., Polak, C., & Stroud, D. (1986). The Behaviour of Single-Lap Bolted Joints in CFRP Laminates. *Composite Structures*, 41-55.
- Tekalur, A. S., VanderKlok, A., Zhang, W., & Dutta, A. (n.d.). Evaluating Bolted Joint Strength at High Strain Rates . *Society of Experimental Mechanics*. Costa Mesa: in press.
- Wang, H.-S., Hung, C.-L., & Chang, F.-K. (1996). Bearing Failure of Bolted Composite Joints. Part 1: Experimental Characterization. *Composite Materials*, 1284-1313.
- Yan, Y., Wen, W.-D., Chang, F. -K., & Shyprykevich, P. (1999). Experimental Study on Clamping Effects on the Tensile Strength of Composite Plates with a Bolt-Filled Hole. *Composites*, 1215-1229.

**Chapter 4 Metal to Composite Bolted Joint Behavior Evaluated at Impact Rates of
Loading**

4.1 Abstract

Characteristics of metal to composite bolted joints loaded at high strain rates are widely unidentified within the bolted joint community. There still remains uncertainty in the investigation of bolting two dissimilar materials together as well as investigation of dissimilar materials under impact loading conditions. It has been proven that in many automotive, marine, and aeronautical applications, composites show superior characteristics to metals under given circumstances. However, the two are commonly used together to provide an optimum design for a particular application. An experimental study showing how two dissimilar materials behave when bolted will be investigated at high rates of loading using a split Hopkinson tension bar (SHTB) and equivalently compared to statically loaded. The hypotheses validated are that the asymptotic region of failure mode alteration is dependent on loading rate transfer. This study provides beneficial information in assisting subsequent design of bolted joints where behavior under impact loading is of main concern.

Keywords: Bolted joint, Split Hopkinson Tension Bar, Failure Mode, Loading Rate Transfer

4.2 Introduction to Dissimilar Material Fastening

Bolting components together is essential in the design of machine components, automobiles, aircraft, and other structures. Bolting components allows for the nondestructive disassembly of components for maintenance, repair, and proves to be sufficient in strength. It has been shown that in many applications, there exist an asymptotic region where mode of failure abruptly changes for varying geometries. This asymptotic behavior is consistent for similar geometric parameters of varying materials. The asymptotic failure behavior shown in [**Kretsis & Matthews, 1985**], [**Smith, Pascoe, Polak, & Stroud, 1986**],[**Godwin & Matthews, 1980**]

implies that under static loading conditions a bolted joints failure mode is highly dependent upon the geometry of the joint. The demand for use of composite materials such as fiber glass yields hybrid designs consisting of both metallic and composite materials alike. The investigation of how dissimilar materials behave with respect to each other is crucial in the successful design where impact rates of loading is a major concern.

4.3 Materials and Methods

Static loading was accomplished with a multipurpose MTS insight with 10kN load cell. Pinned and threaded grips were utilized to hold the specimen in position, and 3 specimens of 3 varying geometries were tested in this static configuration including $e/d=1.0, 2.0, 3.0$; $w/d=5.0$, and $t/d=0.36$ yielding a total of 9 tests. The test was conducted at a loading of 1.5 mm per minute and results recorded. The same tests were conducted with a Split Hopkinson pressure bar with an average loading rate of approximately 100MN/s. The composite specimen is a composite E-glass ply with an epoxy resin commercially obtained from ACP Composites. The metallic portion of the bolted joint was selected to be a multipurpose 4142 alloy steel purchased from McMaster Carr to resist compliance during testing.

To achieve the high loading rates associated with impact rates of loading similar to experienced in car crashes or ballistic impact, the Split Hopkinson tensile bar was utilized shown in **figure 4.1**. The bar uses pressurized helium to accelerate a 5.0 inch striker two inches in diameter to impact the anvil at the end of the incident bar. This induces both a compressive and tensile wave, as well as pulse elongation due to a paper pulse shaper used at the interface of the anvil and striker. A thin anvil is used to achieve high strain amplitude to ensure that specimen failure occurs. The 5/8 inch diameter 10 foot long incident bar is made of 6061-T6 Aluminum and

outfitted with two diametrically opposing EA-13-250-BG electro-resistive strain gages outfitted to an Ectron 835 amplifier configured in a half bridge configuration to eliminate bending and amplify axial strain. The end of the incident bar is tapped with $\frac{1}{2}$ -20 threads to accept a steel grip for the metallic specimens to be pinned and glued. The 1045 steel transmission bar 5 feet in length is equipped with similar tapped $\frac{1}{2}$ -20 threads that accepts a grip shown in **figure 4.1** (bottom) where the specimen is gripped with 5 bolts centered at 2.5 times the bolt diameter with respect to each other. The metallic specimen is reverse dog bone shaped to reduce testing mass and bolted to the specimen with 30 in-lbs of torque shown in **figure 4.1** at the incident side of the setup. This torque was selected as it provides pretension of the bolt that does not exceed the compressive strength of the glass composite. The strain gage cluster is adhered 15 inches from the specimen end of the transmission bar and configured into a full bridge configuration for amplified sensitivity of strain in the axial direction and cancellation of bending strains.

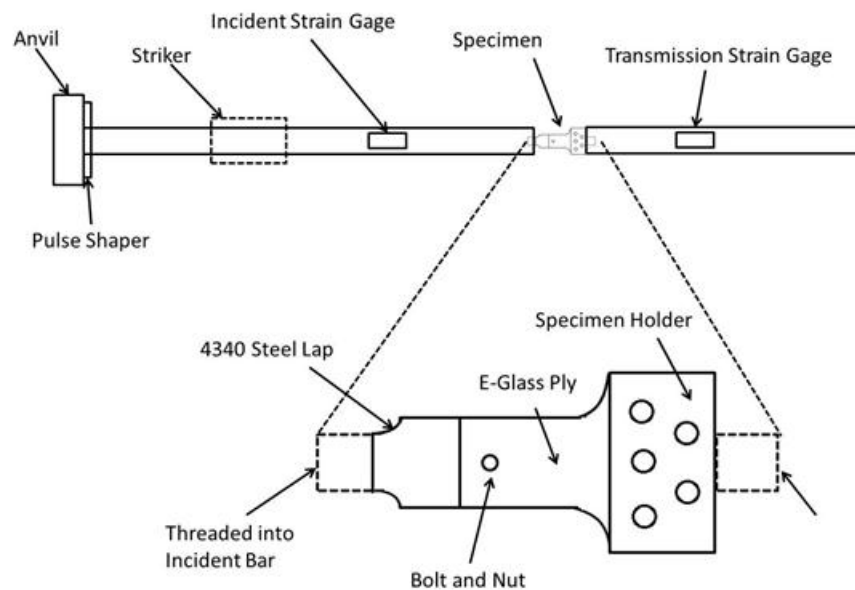


Figure 4.1 Split Hopkinson tension bar apparatus setup (top) and the specimen setup with holding fixtures (bottom)

Three specimens of each configuration were tested in tension statically on the MTS with the following parameters shown in **table 4.1** below. Then another set of identical specimens to that described in **table 4.1** were tested at impact rates of loading. Specimens were attached via a nut and bolt which was torqued to 30 in-lbs. to be careful not to overcome compressive and interlaminar shear stresses of the material [**Matthews, Wong, & Chryssafitis, 1982**].

Table 4.1 Specimen non-dimensional parameters

Specimen Type	e/d	w/d	d/t	l/d	Bolt Preload (in-lbs.)
1	1.00	5.00	0.36	9.60	30
2	2.00	5.00	0.36	8.60	30
3	3.00	5.00	0.36	7.60	30
4	4.00	5.00	0.36	6.60	30

4.4 Results and Discussion of Failure Modes Observed

All specimens that were tested statically and dynamically in this experiment were tested to failure. Failure for this article is defined as when the specimen will no longer hold any bearing force at the joint due to sudden load loss of the composite because of its brittle behavior of the glass composite. Typical specimen failure modes include tension, cleavage, shear out, and bearing as well as any combination of the four shown in **Figure 4.2** [**Bickford, 1990**].

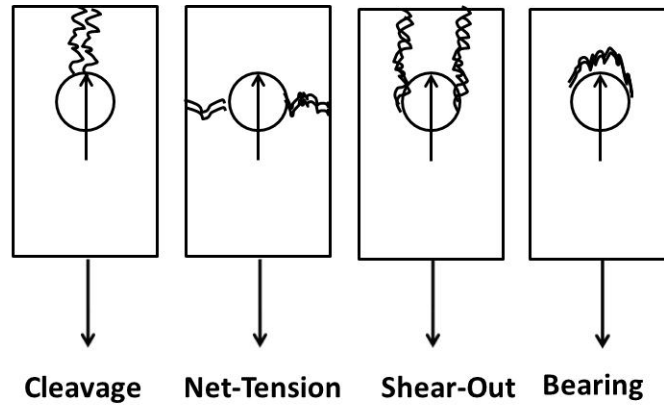


Figure 4.2 Possible Failure modes of a loaded bolted joint loaded at the hole

Specimens were first tested at a tensile rate of 1.5mm/min with an MTS (10kN load cell) at the various geometries provided in table 1 for specimen type of 1, 2, and 3. Specimen type of 4 was not needed for static testing as maximum bearing stress was attained for this particular material and geometry at type 3. A set of stress displacement curves for the 3 different specimens are shown in **figure 4.3** where clearly three different regions exist of initial loading, slip, and bearing load to failure. It can be seen that for the e/d ratio of 2.0 and 3.0 in **figure 4.3**, maximum bearing stress is attained and the curve general behavior does not change rendering subsequent samples with larger e/d ratios unnecessary.

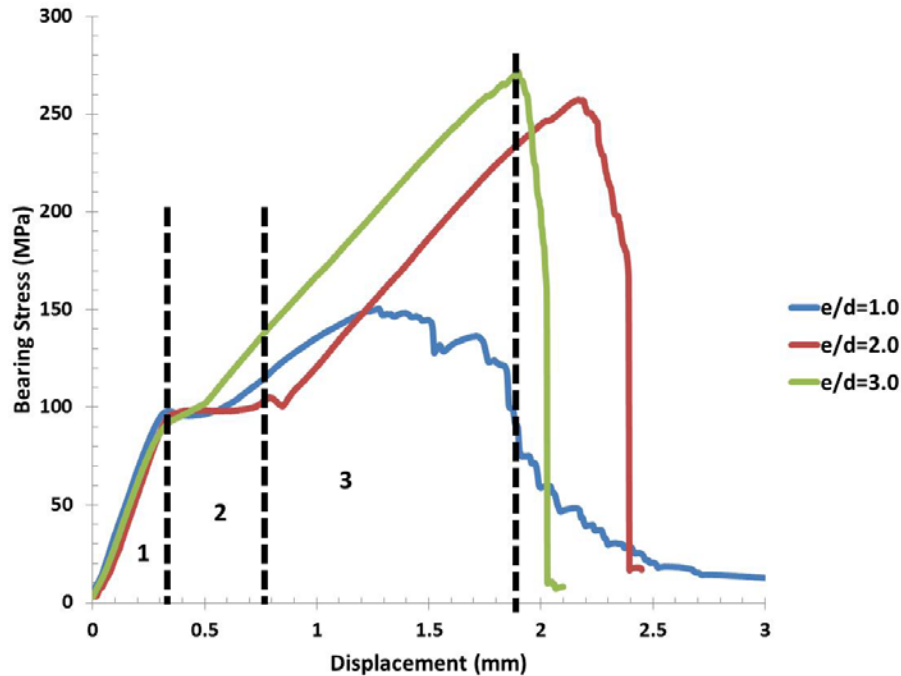


Figure 4.3 Bearing stress vs. displacement curves for bolted joints tested in tension at 1.5mm/min with region 1, 2, and 3 respectively correlating to initial loading, slip, and bearing load to failure.

4.5 Specimen static load bearing characteristics

The main behaviors to notice with the statically loaded specimens is the three main regions the curves can be separated as seen in **figure 4.3** into regions of initial loading, slip, and bearing load to failure. Region 1 behavior shows the load has not exceeded the frictional force of the jointed materials. In this particular case the E-glass composite vs. the 4142 alloy, where the two mating surfaces contain a coefficient of friction that is dependent upon the bolt preload and decays away from the bolt hole [**Groper, 1985**]. Within region 1, linear loading is observed as the joint resist slipping caused by the preload on the bolt caused by torquing the bolt and nut together. Region 2 initiates from exceeding the frictional force and a constant steady load is observed for all

specimen types regardless of contact area in that the bearing stress in the specimen remains constant for differing overlap areas, but same bolt preloads of 30 in-lbs. The joint slip displacement varies from each specimen due to the oversize hole drilled and manner to which the joint was assembled. If the joint was assembled slightly off centered toward the loading side a minimal amount of slipping will be observed and the joint will begin to be loaded in bearing from the bolt as depicted in region 3.

4.6 Specimen dynamic load bearing characteristics

Bolted joints with a set bolt preload show an increase in bearing strength for composites by suppressing delamination of subsequent layers of composite in the out of plane direction [Kelly & Hallstrom, 2003], [Stockdale & Matthews, 1976], [Kong & Kong, 1995], [Park, 2001]. Similarly to increasing bolt preload, increasing loading rate of the bolted joint shows similar characteristics for specimens loaded in tension. High loading rates are achieved with utilizing the SHTB experimental setup. Where, **equation 4.1** is used to determine the force that has been transmitted through the specimen F_{trans} , utilizing known parameters of cross-sectional area of the transmission bar $A_{trans,bar}$, modulus of the transmission bar E_{bar} , and transmitted strain as a function of time $\epsilon(t)$ recorded from the transmitted strain pulse. **Equation 4.2** defines the max bearing stress $\sigma_{bearing, max}$ located on the shear plane of the bolted joint hole, and bearing area $A_{bearing}$ of the shear plane. The max bearing stress is determined from selecting the max transmitted force before failure.

$$F_{trans}(t) = A_{trans.bar} E_{bar} (\epsilon(t)) \quad 4.1$$

$$\sigma_{bearing, max} = \frac{F_{trans,max}}{A_{bearing}} \quad 4.2$$

General trends of maximum bearing stresses in the specimen with geometries listed in **Table 4.1** increases from the static loaded joints shown in **figure 4.4** agree with results found in [Daimaruya, Fujiki, & Uemura, 2009]. The increase in strength of the bolted joint can be attributed to material strain rate sensitivity and inertial effects in the dynamic failure process [Birch & Alves, 2000].

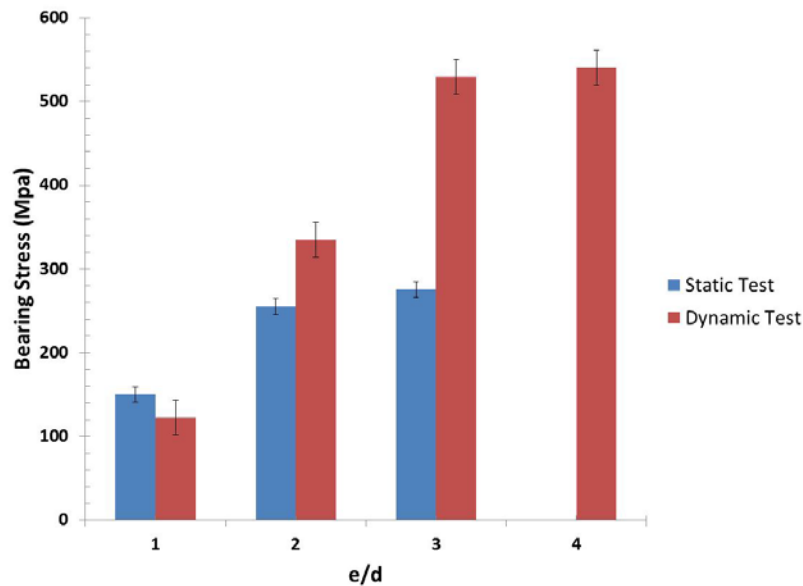


Figure 4.4 static and impact loaded samples compared with maximum bearing stress before catastrophic failure

However, looking at the rate of load transfer to the composite link of the bolted joint, it is clear that the amount of overlap or e/d ratio has a clear dependency seen in **Figure 4.5**. The increasing overlap area of the bolted joint allows for the increase of load transfer rate linearly until the asymptotic region of failure is reached for the specimen geometry. From [Groper, 1985] the coefficient of friction is dependent upon the contact properties which vary during slipping. However, as the rate of load transfer increases in the joint testing the coefficient of friction will increase yielding an increase in maximum bearing strength. In addition to the increase of bolted

joint strength caused by material strain rate sensitivity and inertial effects, the load transfer rate also attributes to the maximum strength of the joint as explained.

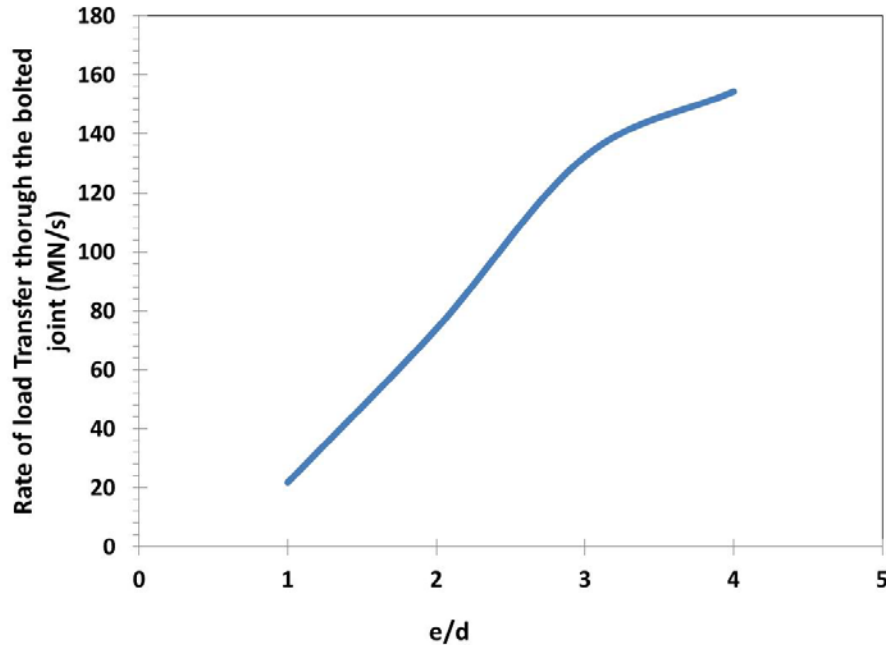


Figure 4.5 Rate of load transfer to the composite bolted joint

4.7 Failure modes of static and dynamically loaded bolted joints

High speed images captured with a phantom high camera at a rate of 100,000 frames per second were used to record the event of the bolted joint as it was loaded with a time dependent load at impact rates. These images are calibrated to the start time of the event and can be correlated with the transmitted pulse generated in the SHTB setup. This allows for direct comparison of the specimen with the load that is transferred to the transmission bar. In addition, for many of the test conducted statically and under impact loads show mixed modes of failure and a strong dependency on joint geometry. The high speed images taken allow for the deduction of failure mode sequence and correlation to how load is transferred to the transmission bar. **Figures 4.6, 4.7, 4.8, and 4.9** show the load transfer curve and correlating failure mode images for the metal

composite joints tested with $e/d=1.0, 2.0, 3.0,$ and 4.0 respectively. It is interesting to note that for the tensile mode of failure does not always propagate from the minimum net area of the plate as expected. This behavior is theoretically explained by [Jong, 1977] where hole clearance to the loading pin is the main culprit for the reason of the maximum stress development away from the minimum net plate area.

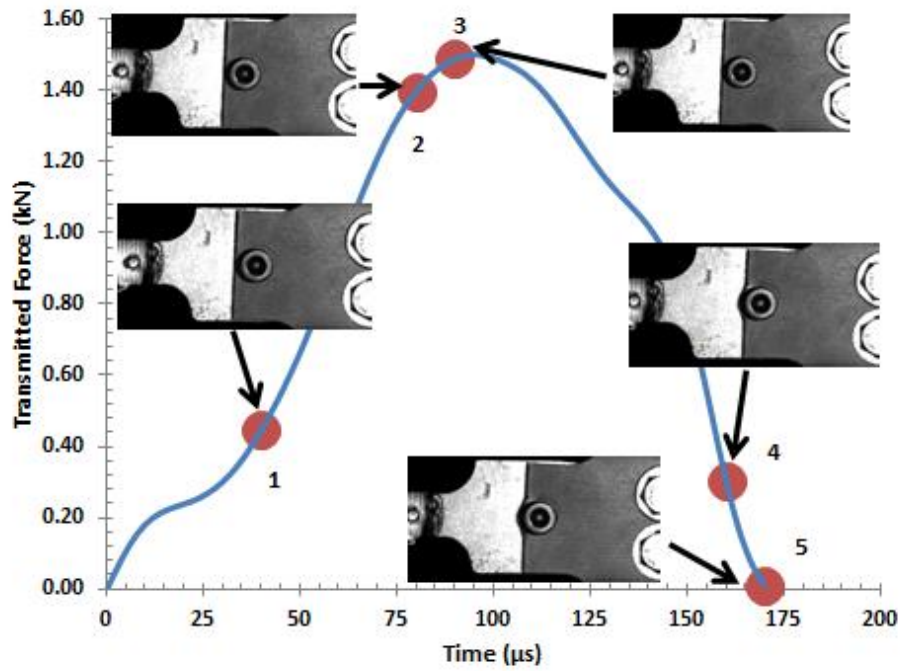


Figure 4.6 Load transfer curve and correlating failure mode images for the metal composite joints tested with $e/d=1.0$

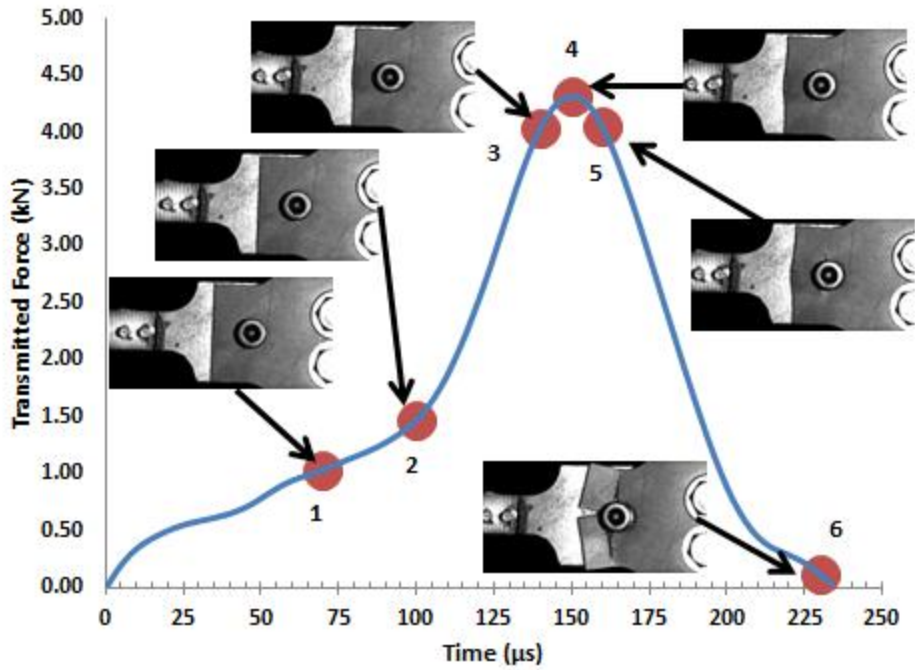


Figure 4.7 Load transfer curve and correlating failure mode images for the metal composite joints tested with $e/d=2.0$

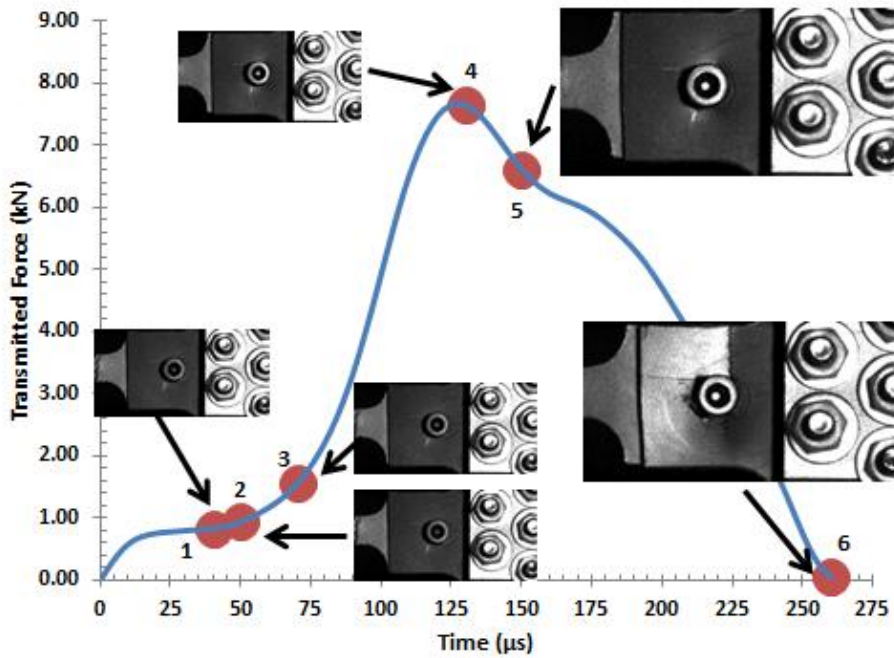


Figure 4.8 Load transfer curve and correlating failure mode images for the metal composite joints tested with $e/d=3.0$

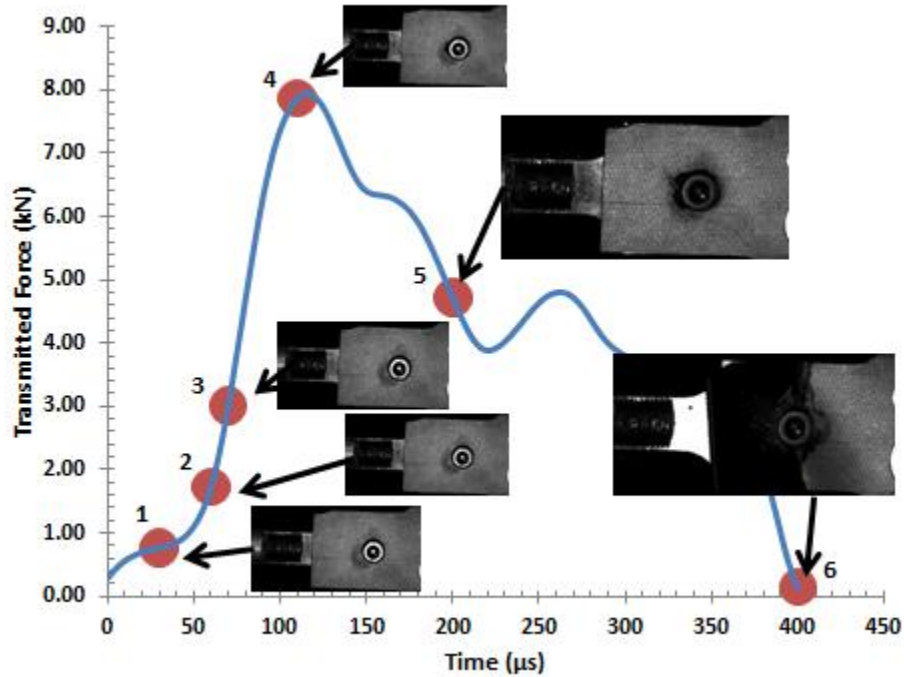


Figure 4.9 Load transfer curve and correlating failure mode images for the metal composite joints tested with $e/d=4.0$

The failure modes for each e/d ratio are unique in that many show a mixed mode failure and a summary of **figures 4.6, 4.7, 4.8, and 4.9** shown in **table 4.2** are given. For the specimens tested the load transfer curve tends to elongate with the increasing overlap area as more time is required to bring the specimen to complete failure.

Table 4.2 Summary of failure mode time initiation

e/d	Number correlating to curve						Figure #
	1	2	3	4	5	6	
1.0	Friction loading up to 40 μ s	Slip and grip compliance @ 80 μ s	Initiation of cleavage failure @ 90 μ s	Initiation of shear-out failure @ 160 μ s	Complete shear-out failure @ 170 μ s		6
2.0	Friction loading up to 70 μ s	Slip and grip compliance @ 100 μ s	Specimen bearing loading @ 140 μ s	Initiation of tension failure @ 150 μ s	Initiation of cleavage failure @ 160 μ s	Complete failure of tension and cleavage @ 230 μ s	7
3.0	Friction loading up to 40 μ s	Slip and grip compliance @ 50 μ s	Specimen bearing loading @ 70 μ s	Bearing damage initiation @ 130 μ s	Tensile failure initiation @ 150 μ s	Complete tensile failure @ 260 μ s	8
4.0	Friction loading up to 30 μ s	Slip and grip compliance @ 60 μ s	Specimen bearing loading @ 70 μ s	Bearing damage initiation @ 110 μ s	Tensile failure initiation @ 200 μ s	Complete tensile failure @ 400 μ s	9

Statically loaded joints the failure modes ultimately reach an asymptote where only one dominant mode of failure and bearing strength exist for increasing edge distance of the specimen. Joints loaded at high rates of strain perform similarly with an increase in bearing stress and geometrical shift as to where the dominant mode of failure will exist. **Figure 4.10** shows these comparisons and it can be seen that the failure modes from the statically loaded specimens differs from the dynamic test. Noting that for statically and dynamically loaded joints, the dominant modes of failure converge to that of tension. These modes of failure build an asymptote for static and dynamically loaded joints, which occurs at e/d=2.0 and 3.0 respectively.

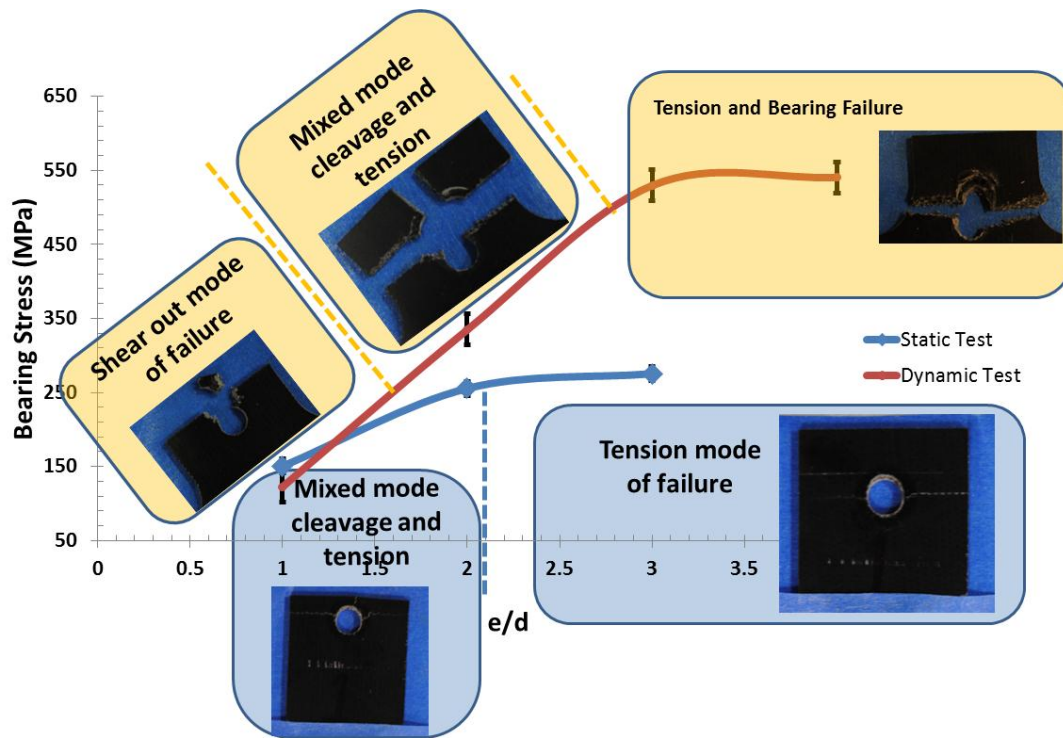


Figure 4.10 Asymptotic failure behavior of bolted joints loaded in tension

The dynamic testing shown in **figure 10** is a compilation identically loaded joints varying only in geometry. With the pulse shaping technique as well as pressure used for the gas gun, dynamic test impact pulse loading rates of 1100 MN/s were achieved with a precision of $\pm 5\%$. The impact pulse loading rate is dissimilar than what is depicted in **Figure 4.5**, rate of load transfer. The rate of load transfer differs for varying joint geometry, and is a pseudo measurement of how efficient the joint performs under the initial impact pulse. This efficiency is a measure of how close the joint comes to transmitting all of the given impact pulse load and is dependent upon geometry, material composition and minimally on bolt preload. Typical losses in efficiency are associated with: failure of the structure where there is crack or delamination development and from relative slip of the two bolted members. From the findings of the previous chapter, the bolt preload has minimal effect on transmitting the impact pulse through the joint. Where the rate of load transfer

is highly dependent upon the joint geometry, rendering why the current study does not vary the bolt preloads. **Figure 4.5** shows a steady increasing behavior of loading rate as the edge diameter is moved further away from the edge of the joint. However, at $e/d=3.0$ begins to plateau as a sign that the joint has reached its maximum load transmitting capability. So, for a designer the curves shown in **Figure 4.5** and **4.10** will allow for optimum joints to be constructed for a given application that may be impact loaded. Further development of lesser loading rates would be beneficial as this would build intermediate curves between that of the static load and dynamic loads allowing for designers to more closely imitate the actual loading rates that would be encountered.

4.9 Conclusion

Specimens tested statically show three main regions of failure: initial loading, slip, bearing load to failure. As joint overlap length is increased with increasing e/d ratios an asymptotic region of maximum bearing strength is attained as well as a dominant mode of failure of tension. Specimens loaded at impact rates of loading were mostly shown to attain higher max bearing stresses. The increase in bearing strength can be attributed to: material strain rate sensitivity, inertial effects, and the load transfer rate caused by material overlap. Modes of failure from the static tests show asymptotic behavior where a dominate failure mode exists after $e/d=2.0$. It was shown that modes of failure are dependent upon loading rate as there was an apparent shift from the asymptotic behavior of $e/d=2.0$ for static to $e/d=3.0$ for dynamic. At impact rates of loading, bolted joints behave differently in bearing strength and mode of failure, which should be considered when designing structures that may undergo time dependent rates of loading.

A future scope of work includes a phenomenological study of hybrid dissimilar material joining at impact rates of loading. Although hybrid joining does not allow for nondestructive disassembly of the joint, it does surpass bolted joints in strength rendering further study into this subject significant.

4.9 References

- Bickford, J. H. (1990). *An Introduction to the Design and Behavior of Bolted Joints*. New York: Marcel Dekker, Inc.
- Birch, R., & Alves, M. (2000). Dynamic Failure of Structural Joint Systems. *Thin-Walled Structures*, 137-154.
- Daimaruya, M., Fujiki, H., & Uemura, Y. (2009). Impact Behavior and Fracture of Jointed Steel Plates. *DYMAT* (pp. 867-873). Muroran: EDP Sciences.
- Godwin, E., & Matthews, F. (1980). A Review of the Strength of Joints in Fibre-Reinforced Plastics. *Composites*, 155-160.
- Groper, M. (1985). Microslip and Macroslip in Bolted Joints. *Experimental Mechanics*, 171-174.
- Jong, T. D. (1977). Stresses Around Pin Loaded Holes in Elastically Orthotropic or Isotropic Plates. *Composite Materials*, 313-331.
- Kelly, g., & Hallstrom, S. (2003). Bearing Strength of Carbon Fibre/Epoxy Laminates: Effects of Bolt-Hole Clearance. *Composites*, 331-343.
- Kong, A. M., & Kong, A. M. (1995). Bearing Strength of Autoclave and oven cured kevlar/epoxy laminates under static and dynamic loading. *Composites*, 451-456.
- Kretsis, G., & Matthews, F. (1985). The Strength of Bolted Joints in Glass Fibre/ Epoxy Laminates. *Composites*, Volume 16. No 2.
- Matthews, F., Wong, C., & Chryssafitis, S. (1982). Stress Distribution around a Single Bolt in Fibre-Reinforced Plastic. *Composites*, 316-322.
- Park, H. (2001). Effects of stacking sequence and clamping force on the bearing strength of mechanically fastened joints in composite laminates . *Composite Structures*, 213-221.
- Smith, P., Pascoe, K., Polak, C., & Stroud, D. (1986). The Behaviour of Single-Lap Bolted Joints in CFRP Laminates. *Composite Structures*, 41-55.
- Stockdale, J., & Matthews, F. (1976). The Effect of Clamping Pressure on Bolt Bearing Loads in Glass Fibre-Reinforced Plastics. *Composites*, 34-38.

Chapter 5 Conclusion

5.1 Concluding Remarks

Bolted joints are extensively used in many automotive and aeronautical sectors where two members are bolted together. Since, bolted joints constitute an integral part of many structural components; this directly implicates the necessity to investigate the mechanical response of the bolted joints under a variety of loading rates to ensure structural integrity.

The present studies aims at investigating and characterizing dynamic mechanical behavior of bolted joints and the role of the non-dimensional parameters affecting joint failure along with bolt preload. The Split Hopkinson Pressure Bar technique has been employed to describe bolted joint failure under impact rates of loading for both compression and tensile loading conditions. Hole elongation and buckling are the key modes of failure under dynamic compressive loading conditions, whereas tear-out, tension, and cleavage failure constitutes the predominant failure modes under dynamic tensile loading conditions. Aluminum-Aluminum and Aluminum-Glass fiber reinforced composite bolted joints were tested under dynamic compression and tension respectively. An experimental method was developed for measuring and monitoring the response to the bolt preload during impact. It was determined that the asymptotic region of failure is variably dependent upon loading rate rendering the importance of further investigating bolted joint behavior at impact rates of strain.

5.2 Future Scope of Work

A future scope of work includes a phenomenological study of hybrid dissimilar material joining at impact rates of loading. Although hybrid joining does not allow for nondestructive disassembly of the joint, it does surpass bolted joints in strength rendering further study into this

subject significant. Again utilizing the split Hopkinson tension bar would allow for the development of a relationship between failure modes of the joint for different loading rates as well as joint geometries. The hybrid joining experiment could be directly compared to the non-hybrid joining methods to validate the hypothesis that bolted and bonded hybrid joints would prove superior in bearing strength.

Appendix

Appendix A Wire and Strain Gage Installation Notes

Strain gages were installed on the Hopkinson bars with soldering tabs that strains caused by pretension from the wires. The installation process recommended from the manufacturer was followed closely along with the use of a GA-2 epoxy for adhering the gages. The GA-2 epoxy is capable of elongations of 6% at 6 hours and 10% after 40 hour cure times. The GA-2 was found to be considerably more durable and reliable for the high strain and strain rate induced in the incident bar and performed superior to that of the M-bond 200 cyanoacrylate based adhesive. Two different strain gages were used on the Hopkinson bars depending on the material type of the bars. Gage EA-13-250BG-120 for Aluminum and EA-06-250BG-120 for steel bars. Shielded 22 gage 2 pair wire was used to complete the circuitry from the Ectron amplifier to the gages. Radio noise caused by nearby large running electrical motors rendered it extremely necessary to shield all wires to significantly reduce noisy signals recording during an experiment.

Appendix B Trigger Mechanisms and Phantom High Speed Camera

For the Hopkinson bar experiments, the impact event is approximately 800 μ s incident, reflected, and transmitted pulses to be recorded. The phantom high speed camera (model v12.0) serves both as a data acquisition tool and power supply used for the trigger switch. The triggers switch is made of a thin diameter graphite rod that shorts the circuit, when broken simultaneously triggers the oscilloscope and camera to begin recording. This is useful in that the incident, reflected, and transmitted pulses generated can be directly correlated to specimen images.

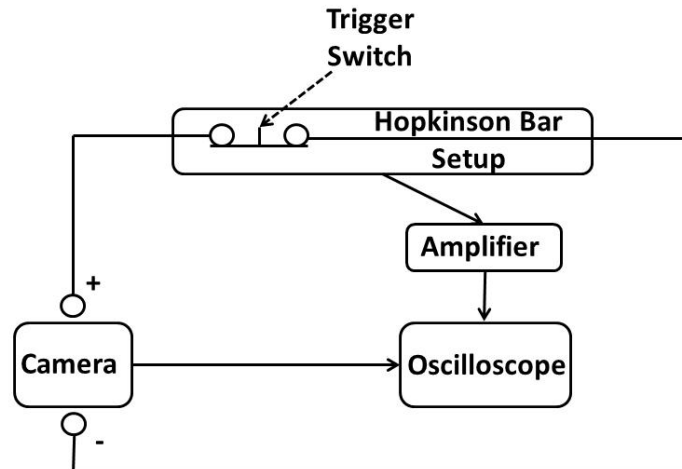


Figure AB1 Flow schematic of equipment for Hopkinson bar data acquisition and high speed capture calibration

Appendix C Ectron 513-2A Amplifier and Calibration and Notes

The Ectron amplifier and enclosure allows for the customization of shunt resistance and Wheatstone Bridge configurations. The shunt resistor is used to calibrate the circuitry to yield a sensitivity factor in values in units of strain per volt. Whereas only voltage values are recorded via the oscilloscope, the sensitivity factor is used to determine the strain. Ideally the shunt resistor, when activated bypasses part of the bridge circuitry and will induce a known imbalance in the bridge. This imbalance is directly related to a known calculated strain value. Values for the shunt calibration resistor are calculated with **equation AB1**, where R_c is the shunt calibration resistor, R_g is the strain gage resistance, F_g is the gage factor of strain gage used, and ϵ_s is a strain value selected. The strain value selected should be an approximate experimental expected strain value, in that this will help to attain maximum sensitivity.

$$R_c = \frac{R_g}{F_g \epsilon_s} - R_g \quad \text{AB1}$$

A Wheatstone bridge is a circuit that contains known and variable resistances of which when altered unbalance the bridge. The circuit is ideal for measuring small amounts of resistance

changes such as that produced by inducing strain on an electro-resistive strain gage, which is why it was chosen for the impact testing using the split Hopkinson pressure and tension bar apparatus (SHPB & SHTB). The Ectron amplifier allows for $\frac{1}{4}$, $\frac{1}{2}$, or full bridge configurations and high acquisition rate. For this application the half bridge configuration and full bridge configuration are used depending on the experimental setup and what type of strain is to be measured. It should be noted that with Hopkinson bar testing noisy signals can arise from more than just local electromagnetically induced voltages, but bending as well. The bars are aligned as closely as possible however due to small imperfections in the straightness of the bars and alignment of the striker and incident bar, the bar will experience some degree of bending strain. This can be cancelled out with two strain gages placed diametrically opposing and the average strains will yield only axial strain. This proves to be tedious, time consuming and less sensitive compared to other configurations.

The half bridge configuration shown in **figure AC1** is utilized for the incident bar on the SHPB. A half bridge configuration is chosen in that it gives good sensitivity, however can be configured as shown in **figure AC1** to be sensitive to axial strain and insensitive to bending strains, only if the gages are installed diametrically opposing each other and wired as shown in **figure AC2**.

Figure AC3 shows the gage positioning on the bar for the full bridge configuration. This configuration is special in that it has the best sensitivity to axial strains, and very little sensitivity to bending strain. The schematic of the full bridge configuration is shown in **figure AC4**. Each of the gage configurations are summarized in **Table AC1**.

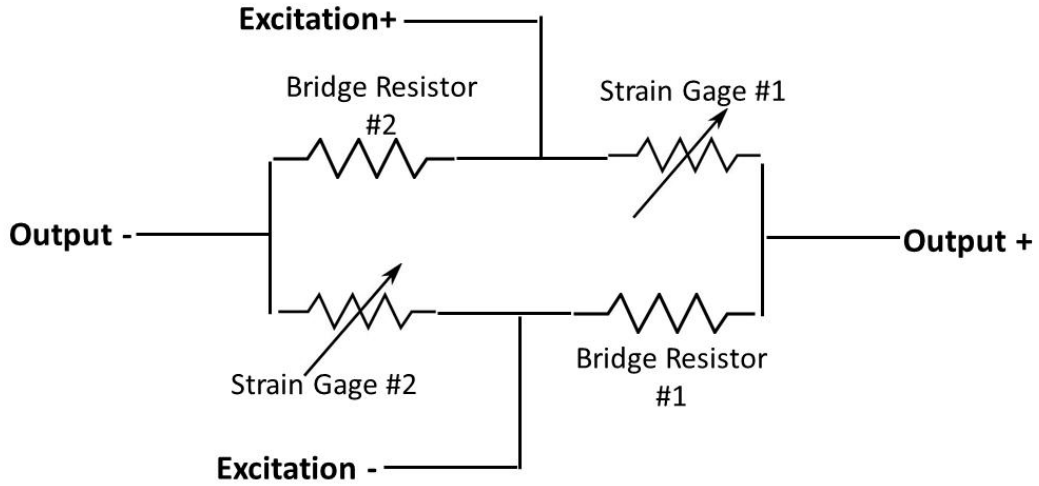


Figure AC1 1/2-Wheatstone bridge circuit

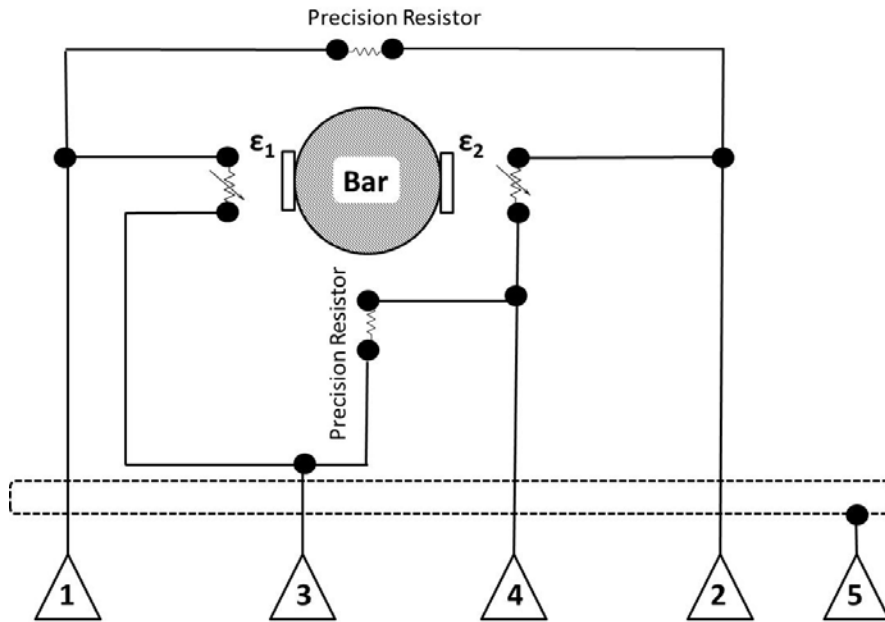


Figure AC2 1/2-Wheatstone bridge Hopkinson incident bar schematic, where numbers in triangles represent pin connection in Ectron 513-2A enclosure

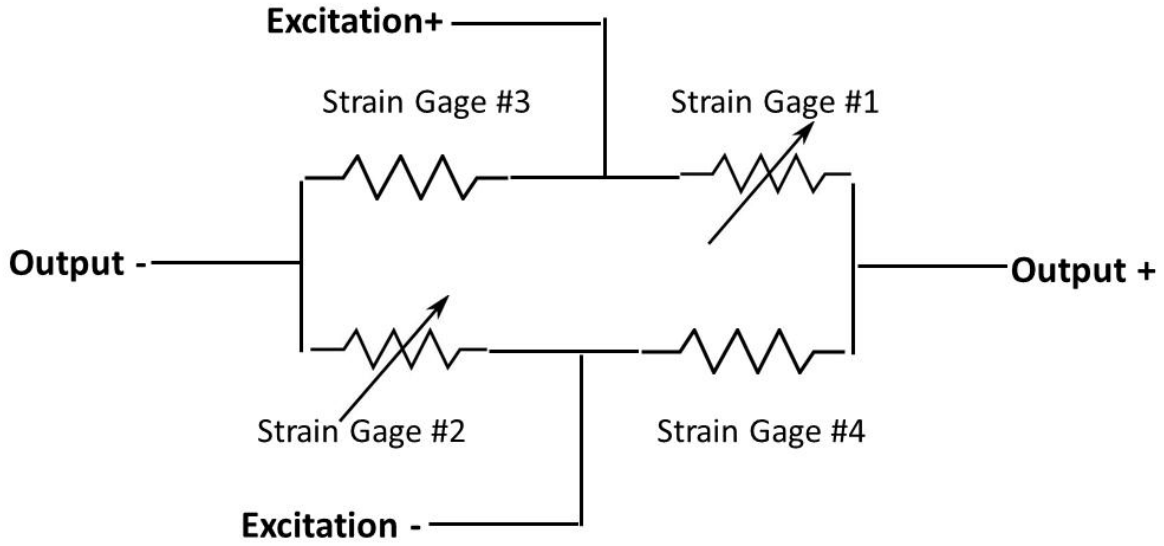


Figure AC3 Full Wheatstone bridge circuit

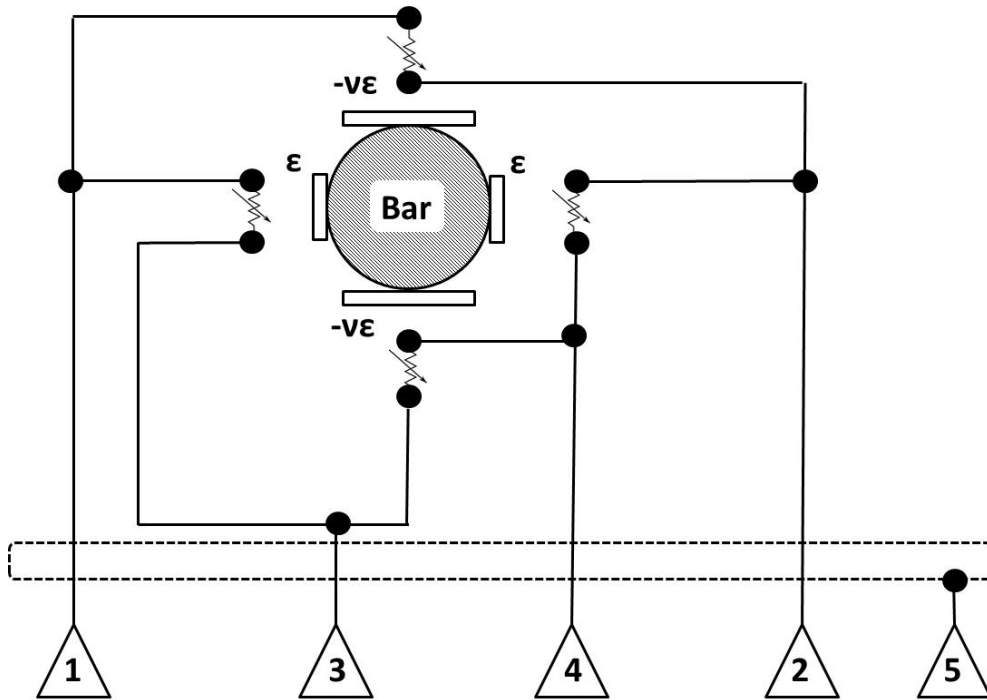


Figure AC4 Full Wheatstone bridge Hopkinson transmission bar and load cell schematic, where numbers in triangles represent pin connections in Ectron 513-2A enclosure

Table AC1 Characterization of bridge configuration and sensitivity, where better sensitivity signifies a smaller ratio of $\mu\epsilon/\text{Volt}$

Bridge Configuration	Sensitivity ($\mu\epsilon/\text{Volt}$)	Notes
quarter	100.00	Poor sensitivity, no cancellation of bending strain
half	50.00	Moderate sensitivity, cancellation of bending strain and reduction of RF noise from electrical machinery
full	25.00	Best Sensitivity Cancellation of bending and reduction of RF noise from electrical machinery